The free vibration of the MEE sandwich microplate with the FG-CNTRC core using the MSGT

*T. T. Trien , P. T. Hung**
Faculty of Civil Engineering, Ho Chi Minh City University of Technology and Education, Ho Chi Minh City, Vietnam.

*Corresponding Author: P. T. Hung (email: hungpht@hcmute.edu.vn)
(Received: 09-May-2024; accepted: 15-July-2024; published: 30-September-2024)
http://dx.doi.org/10.55579/jaec.202483.463

Abstract. *This study deals with the free vibration of the sandwich microplate with the core made of functionally graded carbon nanotube-reinforced composites (FG-CNTRC) and magneto-electro-elastic (MEE) face sheets. The governing equation of the microplates is derived by using the refined plate theory (RPT) with two variables and the modified strain gradient theory (MSGT). The Non-Uniform Rational B-Splines (NURBS) basis function of the isogeometric approach (IGA) is used for the approximation of the displacement and electric and magnetic fields of the microplates. The paper studies the effect of the length scale parameters (LSPs), CNTs distributions, CNTs volume fraction, magnetic and electric loads and geometry on the vibrational frequency of the MEE sandwich microplate.*

Keywords: *Isogeometric approach, magneto-electro-elastic, modified strain gradient theory, functionally graded carbon nanotube-reinforced composites.*

1. Introduction

The modified strain gradient theory (MSGT) is an enhanced framework in material science, refining traditional strain gradient theories to capture finer details of material behavior. By incorporating higher-order strain gradients, this theory addresses limitations in classical models, particularly in micro and nanoscale applications, offering improved accuracy in predicting material responses under complex conditions. Lam et al. [1] firstly presented a MSGT incorporating three length-scale parameters (LSPs). According to the MSGT the size-dependent of the micro structures were studied by many scientists. Examining static bending and free vibration of a piezoelectric microbeams subjected to mechanical and electric loads, Li et al. [2] conducted their study based on the Timoshenko beam theory and MSGT. The buckling analysis of the rectangular plate was explored by Mohammadi and coworkers [3] utilizing the MSGT and the Kirchoff plate theory (KPT). Hosseini et al. [4] utilized the KPT to analyze the buckling of an orthotropic multi-microplate system positioned on a Pasternak foundation, employing the MSGT. The free vibration of the functionally graded porous (FGP) microbeams was elucidated by Karamanli et al. [5], utilizing both the MSGT and quasi-3D theory. Furthermore, Wang et al. [6] investigated the vibration and static responses of a porous metal foam microbeam by employing the MSGT and sinusoidal beam theory. In their analytical study, Zhang et al. [7] incorporated the MSGT alongside the refined plate theory (RPT) to examine the static, buckling, and free vibration of the FG microplates supported on an elastic medium. Applying the MSGT, Ashoori [8] investigated a geometrically

nonlinear plate formulation using the first-order shear deformation theory and von Karman nonlinear strains. Besides, Le et al. [9–11] formulated a mathematical model for the microstructures based on general Mindlin's strain gradient theory.

Magneto-electro-elastic (MEE) materials are advanced materials that contain the unique capability to integrate mechanical, magnetic and electrical properties. This unique combination makes MEE materials valuable in various applications, including sensors, actuators, and smart devices. For these reasons, many scientists have devoted considerable time to researching the behaviors of the structures made of MEE materials. Liu et al. [12] reported the analytical static and vibration of MEE composite plates with piezoelectric and piezomagnetic layers based on KPT. The investigation of free vibration with large amplitude in MEE laminated plates on an elastic medium was conducted by Shooshtari et al. [13]. This study utilized the analytical method and first-order shear deformation theory (FSDT). Employing Eringen's nonlocal theory and the third-order shear deformation theory (TSDT), combined with analytical approach, Mohammadimehr and coworkers [14] investigated the force vibration, static and buckling of nanocomposite microplates, taking into account MEE properties. Zur and colleagues [15]] utilized the sinusoidal shear deformation theory (SSDT) and nonlocal theory to study the stability and vibration of the FG MEE nanoplates subjected to electrical, mechanical, and magnetic loads. In recent studies, examinations of the dynamic and static of the MEE plates have been documented in [16]. Certain scholars directed their attention towards conducting analyses on the mechanical responses of the FG-CNTRC structures. Shi and colleagues [17], utilizing the FSDT, determined the exact solution for the free vibration of FG-CNTRC beams. Chalak et al. [18] explored the hygrothermal free vibration of FG-CNTRC beams by employing the higher-order zigzag theory and the finite element method (FEM). Zghal and coworkers [19] presented the FEM to introduce the static bending of the FG-CNTRC structures, encompassing plates and shells. Duc et al. [20] presented the free vibration analysis of the FG-CNTRC plates with cracks based on the FSDT and FEM.

As per the cited references and the author's knowledge, no existing research employs isogeometric analysis (IGA) and the MSGT to explore the free vibration behavior of the sandwich microplates with MEE face sheets and FG-CNTRC core. To study the behavior of the microstructure using MSGT, the analytical methods are beneficial because they allow for the manipulation of higher-order derivatives in the approximate functions of higher-order stress. However, for practical applications involving real structures, numerical techniques like FEM, meshfree methods, IGA, and similar approaches are often the most suitable options. One advantage of IGA is its ability to achieve any desired level of continuity with its basic functions, thus meeting the C^1-continuity requirement of the MSGT microplate model. Hughes and coworkers [21] initially introduced the isogeometric method. References [22–24] discuss the free vibration, bending, and buckling analyses of microplates utilizing the MSGT and IGA. Additionally, Thai et al. [25, 26] applied a joint approach involving MSGT and HSDT to investigate the natural frequencies and deflection of the FG microplates. In addition, the fracture of the FG-MEE plates was studied by Singh et al. [27] using the extended IGA. Kiran et al. [28, 29] employed the IGA to present the brittle fracture in the piezoelectric materials. In this paper, we utilize the refined plate theory incorporating two variables and the MSGT to investigate the free vibration of the sandwich microplates with MEE face layers and FG-CNTRC core under the electric and magnetic loads. The effects of the length scale parameters (LSPs), various types of CNTs distributions, external magnetic and electric loads and geometry on the vibrational frequency of the MEE sandwich microplates are presented.

2. Fundamental equations

2.1. The displacement fields

In this investigation, the RPT with two variables is utilized to represent the displacement fields as

follows:

$$\mathbf{u} = \mathbf{u}_1 + 2\mathbf{u}_2 + f(z)\,\mathbf{u}_3 \tag{1}$$

where

$$\mathbf{u} = \begin{Bmatrix} \overline{u} \\ \overline{v} \\ \overline{w} \end{Bmatrix}; \mathbf{u}_1 = \begin{Bmatrix} 0 \\ 0 \\ w_b + w_s \end{Bmatrix}; \mathbf{u}_2 = -\begin{Bmatrix} w_{b,x} \\ w_{b,y} \\ 0 \end{Bmatrix}; \mathbf{u}_3 = \begin{Bmatrix} w_{s,x} \\ w_{s,y} \\ 0 \end{Bmatrix};$$
$$f(z) = -4z^3/3h^2 \tag{2}$$

where w_b denotes the bending transverse displacement; w_s represents the shear transverse displacement; index "," denotes the differential operator.

The strain tensor is defined by follow

$$\begin{cases} \boldsymbol{\varepsilon}_b = z\boldsymbol{\varepsilon}_1 + f(z)\boldsymbol{\varepsilon}_2 \\ \boldsymbol{\varepsilon}_s = (1 + f'(z))\,\bar{\boldsymbol{\varepsilon}}_s \end{cases} \tag{3}$$

with $f'(z) = \frac{\mathrm{d}f(z)}{\mathrm{d}z}$, and

$$\boldsymbol{\varepsilon}_b = \begin{Bmatrix} \varepsilon_x \\ \varepsilon_y \\ \gamma_{xy} \end{Bmatrix}; \boldsymbol{\varepsilon}_1 = -\begin{Bmatrix} w_{b,xx} \\ w_{b,yy} \\ 2w_{b,xy} \end{Bmatrix}; \boldsymbol{\varepsilon}_2 = \begin{Bmatrix} w_{s,xx} \\ w_{s,yy} \\ 2w_{s,xy} \end{Bmatrix};$$
$$\boldsymbol{\varepsilon}_s = \begin{Bmatrix} \gamma_{xz} \\ \gamma_{yz} \end{Bmatrix}; \bar{\boldsymbol{\varepsilon}}_s = \begin{Bmatrix} w_{s,x} \\ w_{s,y} \end{Bmatrix} \tag{4}$$

In accordance with Maxwell's equation [30], the magnetic (Ψ) and electric (Φ) potentials can be formulated as follows

$$\begin{cases} \Phi(x,y,z) = \varphi(x,y)\,g(z) + \frac{2z\phi_0}{h} \\ \Psi(x,y,z) = \psi(x,y)\,g(z) + \frac{2z\psi_0}{h} \end{cases} \tag{5}$$
$$\text{with } g(z) = \cos\left(\tfrac{\pi z}{h}\right)$$

where (ψ) and (ϕ) are respectively represent the in-plane magnetic and electric potentials. Additionally, (ψ_0) and (ϕ_0) signify the initial external magnetic potential and electric voltage, respectively.

The electric and magnetic fields are defined in accordance with Maxwell's equations by following

$$\mathbf{E} = \begin{Bmatrix} E_x \\ E_y \\ E_z \end{Bmatrix} = -\begin{Bmatrix} \Phi_{,x} \\ \Phi_{,y} \\ \Phi_{,z} \end{Bmatrix} = -\begin{Bmatrix} g(z)\,\varphi_{,x} \\ g(z)\,\varphi_{,y} \\ g'(z)\,\varphi + \frac{2\phi_0}{h} \end{Bmatrix};$$
$$\mathbf{H} = \begin{Bmatrix} H_x \\ H_y \\ H_z \end{Bmatrix} = -\begin{Bmatrix} \Psi_{,x} \\ \Psi_{,y} \\ \Psi_{,z} \end{Bmatrix} = -\begin{Bmatrix} g(z)\,\psi_{,x} \\ g(z)\,\psi_{,y} \\ g'(z)\,\psi + \frac{2\psi_0}{h} \end{Bmatrix} \tag{6}$$

where $\mathbf{E}$ is the vector of electric field, while are the electric field's components; $\mathbf{H}$ denotes the vector of magnetic field, while are the components of the magnetic field.

Based on the MSGT [1], the rotation gradient tensor $\boldsymbol{\chi}$ of the microplate is formulated as follow

$$\boldsymbol{\chi} = \tfrac{1}{2}\left(\nabla\boldsymbol{\theta} + \nabla\boldsymbol{\theta}^T\right) = \begin{Bmatrix} \boldsymbol{\chi}_b \\ \boldsymbol{\chi}_s \end{Bmatrix} = \begin{Bmatrix} \chi_{b1} + f'(z)\,\chi_{b2} \\ f"(z)\,\boldsymbol{\chi}_{s1} \end{Bmatrix};$$
$$\boldsymbol{\theta} = \tfrac{1}{2}\left(\nabla\mathbf{u} - \nabla\mathbf{u}^T\right) \tag{7}$$

where

$$\boldsymbol{\chi}_b = \begin{Bmatrix} \chi_{xx} \\ \chi_{yy} \\ \chi_{xy} \end{Bmatrix}; \boldsymbol{\chi}_s = \begin{Bmatrix} \chi_{xz} \\ \chi_{yz} \end{Bmatrix};$$
$$\boldsymbol{\chi}_{b1} = \frac{1}{4}\begin{Bmatrix} 4w_{b,xy} + 2w_{s,xy} \\ -4w_{b,xy} - 2w_{s,xy} \\ 2w_{b,yy} - 2w_{b,xx} + 2w_{x,yy} - 2w_{s,xx} \end{Bmatrix};$$
$$\boldsymbol{\chi}_{b2} = \frac{1}{4}\begin{Bmatrix} -2w_{s,xy} \\ 2w_{s,xy} \\ w_{s,xx} - w_{s,yy} \end{Bmatrix}; \boldsymbol{\chi}_{s1} = \frac{1}{4}\begin{Bmatrix} -w_{s,y} \\ w_{s,x} \end{Bmatrix} \tag{8}$$

Likewise, the dilatation gradient tensor, as per Eq. 1, assumes the forms:

$$\boldsymbol{\zeta} = \boldsymbol{\zeta}_1 + z\boldsymbol{\zeta}_2 + f(z)\,\boldsymbol{\zeta}_3 + f'(z)\,\boldsymbol{\zeta}_4 \tag{9}$$

where

$$\boldsymbol{\zeta}_1 = -\begin{Bmatrix} 0 \\ 0 \\ w_{b,xx} + w_{b,yy} \end{Bmatrix}; \quad \boldsymbol{\zeta}_2 = -\begin{Bmatrix} w_{b,xx} + w_{b,xy} \\ w_{b,yy} + w_{b,xxy} \\ 0 \end{Bmatrix};$$
$$\boldsymbol{\zeta}_3 = \begin{Bmatrix} w_{s,xx} + w_{s,xyy} \\ w_{s,yyy} + w_{s,xyy} \\ 0 \end{Bmatrix}; \quad \boldsymbol{\zeta}_4 = \begin{Bmatrix} 0 \\ 0 \\ w_{s,xx} + w_{s,yy} \end{Bmatrix} \tag{10}$$

Moreover, the deviatoric stretch gradient tensor is formulated as follows

$$\boldsymbol{\eta} = \begin{Bmatrix} \boldsymbol{\eta}_b \\ \boldsymbol{\eta}_s \end{Bmatrix} = \begin{Bmatrix} z\boldsymbol{\eta}_{b1} + f(z)\,\boldsymbol{\eta}_{b2} + f"(z)\,\boldsymbol{\eta}_{b3} \\ \boldsymbol{\eta}_{s1} + f'(z)\,\boldsymbol{\eta}_{s2} \end{Bmatrix} \tag{11}$$

where

$$\boldsymbol{\eta}_b = \begin{bmatrix} \eta_{\mathrm{xx}} \\ \eta_{\mathrm{yyy}} \\ \eta_{\mathrm{yyx}} \\ \eta_{\mathrm{xy}} \\ \eta_{\mathrm{zx}} \\ \eta_{\mathrm{zy}} \end{bmatrix}; \boldsymbol{\eta}_s = \begin{bmatrix} \eta_{zz} \\ \eta_{\mathrm{xx}} \\ \eta_{\mathrm{yyz}} \\ \eta_{\mathrm{xyz}} \end{bmatrix};$$

$$\boldsymbol{\eta}_{b1}=\frac{1}{5}\begin{Bmatrix}-2w_{b,\mathrm{xx}}+3w_{b,\mathrm{xy}}\\-2w_{b,\mathrm{xy}}+3w_{b,\mathrm{xy}}\\w_{b,\mathrm{xx}}-4w_{b,\mathrm{xy}}\\w_{b,\mathrm{xy}}-4w_{b,\mathrm{xy}}\\w_{b,\mathrm{xx}}+w_{b,\mathrm{xy}}\\w_{b,\mathrm{xy}}+w_{b,\mathrm{xy}}\\w_{b,\mathrm{xy}}+w_{b,\mathrm{xy}}\end{Bmatrix};$$

$$\boldsymbol{\eta}_{b_2}=\frac{1}{5}\begin{Bmatrix}2w_{s,xx}-3w_{s,xy}\\2w_{s,yy}-3w_{s,xy}\\-w_{s,xx}+4w_{s,xy}\\-w_{s,yy}+4w_{s,xxy}\\-w_{s,xx}-w_{s,xyy}\\-w_{s,yy}-w_{s,xy}\end{Bmatrix};$$

$$\boldsymbol{\eta}_{b3}=-\frac{1}{15}\begin{Bmatrix}3w_{s,x}\\3w_{s,y}\\w_{s,x}\\w_{s,y}\\-4w_{s,x}\\-4w_{s,y}\end{Bmatrix};$$

$$\boldsymbol{\eta}_{s1}=\frac{1}{15}\begin{Bmatrix}3w_{b,xx}+3w_{b,yy}-3w_{s,xx}-3w_{s,yy}\\-4w_{b,xx}+w_{b,yy}+4w_{s,xx}-w_{s,yy}\\-4w_{b,yy}+w_{b,xx}+4w_{s,yy}-w_{s,xx}\\-5w_{b,xy}+5w_{s,xy}\end{Bmatrix};$$

$$\boldsymbol{\eta}_{s2}=\frac{1}{15}\begin{Bmatrix}-6w_{s,xx}-6w_{s,yy}\\8w_{s,xx}-2w_{s,yy}\\8w_{s,yy}-2w_{s,xx}\\10w_{s,xy}\end{Bmatrix} \tag{12}$$

where, δ denotes the Kronecker's delta.

2.2. The material properties

Consider the sandwich microplate as illustrated in Figure 1. The microplate's face sheets are fabricated using isotropic magneto-electro-elastic material. Additionally, the core is comprised of an epoxy matrix reinforced with CNTs and includes four distributions: FG-UD, FG-X, FG-O, and FG-V. According to the extended rule of mixture [31], the equivalent material properties of the FG-CNTRC core are formulated as follows

$$\begin{cases}E_{11}^{c}=\eta_1 V_{CNT}E_{11}^{CNT}+V_mE^m;\\E_{22}^{c}=\dfrac{\eta_2}{V_{CNT}/E_{22}^{CNT}+V_m/E^m};\\G_{12}^{c}=\dfrac{\eta_3}{V_{CNT}/G_{12}^{CNT}+V_m/G^m};\\\nu_{12}^{c}=V_{CNT}\nu_{12}^{CNT}+V_m\nu_m;\\\rho^{c}=V_{CNT}\rho_{CNT}+V_m\rho_m\\V_m=1-V_{CNT}\end{cases} \tag{13}$$

in which the symbol 'c' represents the core layer, whereas the symbols 'CNT' and 'm' denote carbon nanotubes and matrix, respectively; E, G, ν, ρ and V respectively denote the Young's modulus, shear modulus, Poisson's ratio, mass density and volume fraction; η_1, η_2 and η_3 represent the CNTs efficiency parameters, which are presented in Table 1. This paper employs four

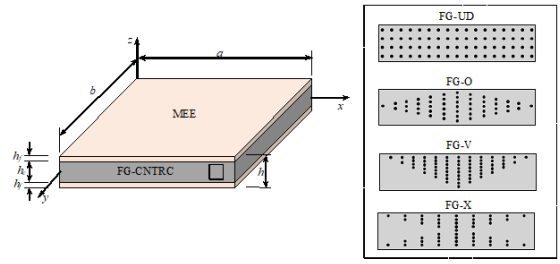

Fig. 1: The geometry of the sandwich microplate.

distribution patterns to enhance the integration of carbon nanotubes across the thickness of the material matrix within the plate. The volume fraction of CNTs in Equation 13 is explained for different CNTs distributions as follows

$$\begin{cases}V_{CNT}=V^* & \mathrm{FG-UD};\\V_{CNT}(z)=\left(1+\frac{2z}{h_c}\right)V^* & \mathrm{FG-V};\\V_{CNT}(z)=\frac{4|z|}{h_c}V^* & \mathrm{FG}-X;\\V_{CNT}(z)=\left(2-\frac{4|z|}{h_c}\right)V^* & \mathrm{FG-O}\end{cases} \tag{14}$$

where

$$V^*=\frac{\rho_m w_{CNT}}{\rho_m w_{CNT}+\rho_{CNT}(1-w_{CNT})} \tag{15}$$

where w_{CNT} is the CNTs mass fraction.

2.3. The constitutive relations

Taking into account the MSGT [1], the constitutive relations of the core layer can be defined

Tab. 1: The CNTs efficiency parameters [32].

V*	η_1	η_2	η_3
0.12	0.137	1.022	0.715
0.17	0.142	1.626	1.138
0.28	0.141	1.585	1.109

as follows

$$\begin{cases} \boldsymbol{\sigma}_b^c = \mathbf{C}_{bc}\boldsymbol{\varepsilon}_b;\ \boldsymbol{\sigma}_s^c = \mathbf{C}_{sc}\boldsymbol{\varepsilon}_s \\ \mathbf{m}_b^c = 2\mu^c l_1^2 \mathbf{I}_{3\times3}\boldsymbol{\chi}_b;\ \mathbf{m}_s^c = 2\mu^c l_1^2 \mathbf{I}_{2\times2}\boldsymbol{\chi}_s; \\ \mathbf{p}^c = 2\mu^c l_2^2 \mathbf{I}_{3\times3}\boldsymbol{\zeta}; \\ \boldsymbol{\tau}_b^c = 2\mu^c l_3^2 \mathbf{I}_{6\times6}\boldsymbol{\eta}_b;\ \boldsymbol{\tau}_s^c = 2\mu^c l_3^2 \mathbf{I}_{4\times4}\boldsymbol{\eta}_s \end{cases} \tag{16}$$

in which

$$\begin{aligned} &\boldsymbol{\sigma}_b^c = \left\{ \begin{array}{cc} \sigma_x^c & \sigma_y^c \end{array} \ \widehat{\tau}_{xy}^c \right\}^T;\ \boldsymbol{\sigma}_s^c = \left\{ \widehat{\tau}_{xz}^c \quad \widehat{\tau}_{yz}^c \right\}^T; \\ &\mathbf{m}_b^c = \left\{ \begin{array}{ccc} m_{xx}^c & m_{yy}^c & m_{xy}^c \end{array} \right\}^T;\ \mathbf{m}_s^c = \left\{ \begin{array}{cc} m_{xz}^c & m_{yz}^c \end{array} \right\}^T; \\ &\mathbf{p}^c = \left\{ \begin{array}{ccc} p_x^c & p_y^c & p_z^c \end{array} \right\}^T; \\ &\boldsymbol{\tau}_b^c = \left\{ \begin{array}{cccccc} \tau_{xxx}^c & \tau_{yyy}^c & \tau_{yyx}^c & \tau_{xxy}^c & \tau_{zzx}^c & \tau_{zzy}^c \end{array} \right\}^T; \\ &\boldsymbol{\tau}_s^c = \left\{ \begin{array}{cccc} \tau_{zzz}^c & \tau_{xxz}^c & \tau_{yyz}^c & \tau_{xyz}^c \end{array} \right\}^T; \\ &\mathbf{C}_{bc} = \begin{bmatrix} C_{11} & C_{12} & 0 \\ C_{12} & C_{22} & 0 \\ 0 & 0 & C_{66} \end{bmatrix};\ \mathbf{C}_{sc} = \begin{bmatrix} C_{55} & 0 \\ 0 & C_{44} \end{bmatrix} \end{aligned} \tag{17}$$

Besides, I_{2x2}, I_{3x3}, I_{4x4} and I_{6x6} respectively denote the 22, 33, 44 and 66 identity matrices; while $\sigma_x^c, \sigma_y^c, \hat{\tau}_{xy}^c, \hat{\tau}_{xz}^c$ and $\hat{\tau}_{yz}^c$ represent the stress components, while $m_{xx}^c, m_{yy}^c, m_{xy}^c, m_{xz}^c, m_{yz}^c$, p_x^c, p_y^c, p_z^c and $\tau_{xxx}^c, \tau_{yyy}^c, \tau_{yyx}^c, \tau_{xxy}^c, \tau_{zzx}^c, \tau_{zzy}^c, \tau_{zzz}^c, \tau_{xxz}^c, \tau_{yyz}^c, \tau_{yyz}^c$ represent the higher-order stress components of the core layer; $C_{11}, C_{12}, C_{22}, C_{44}, C_{55}$ and C_{66} are the elastic coefficients; l_1, l_2 and l_3 denote three LSPs; μ^c represents Lame's coefficient. The definition of the elastic coefficients and Lame's coefficient is presented as follow

$$\begin{aligned} &C_{11} = \frac{E_{11}^c}{1-\nu_{12}^c\nu_{21}^c};\ C_{22} = \frac{E_{22}^c}{1-\nu_{12}^c\nu_{21}^c};\ C_{12} = \frac{\nu_{21}^c E_{11}^c}{1-\nu_{12}^c\nu_{21}^c}; \\ &C_{44} = G_{23}^c;\ C_{55} = G_{13}^c;\ C_{66} = G_{12}^c;\ \mu^c = \frac{C_{44}+C_{55}+C_{66}}{3} \end{aligned} \tag{18}$$

According to the coupling of magnetic, electric, and elastic fields, and employing the MSGT [1], the constitutive relations of the face layers are presented by

$$\begin{cases} \boldsymbol{\sigma}_b^f = \mathbf{C}_{bf}\boldsymbol{\varepsilon}_b - \mathbf{C}_{ueb}\mathbf{E}_b - C_{umb}\mathrm{H}_b \\ \boldsymbol{\sigma}_s^f = \mathbf{C}_{sf}\boldsymbol{\varepsilon}_s - \mathbf{C}_{ues}\mathbf{E}_s - \mathbf{C}_{ums}\mathrm{H}_s \\ \mathbf{D}_b = \mathbf{C}_{ueb}^T\boldsymbol{\varepsilon}_b + \mathbf{C}_{eeb}\mathbf{E}_b + \mathbf{C}_{emb}\mathrm{H}_b \\ \mathbf{D}_s = \mathbf{C}_{ues}^T\boldsymbol{\varepsilon}_s + \mathbf{C}_{ees}\mathbf{E}_s + \mathbf{C}_{ems}\mathrm{H}_s \\ \mathbf{B}_b = \mathbf{C}_{umb}^T\boldsymbol{\varepsilon}_b + \mathbf{C}_{emb}\mathbf{E}_b + \mathbf{C}_{mmb}\mathrm{H}_b \\ \mathbf{B}_s = \mathbf{C}_{ums}^T\boldsymbol{\varepsilon}_s + \mathbf{C}_{ems}\mathbf{E}_s + \mathbf{C}_{mms}\mathrm{H}_s \\ \mathbf{m}_b^f = 2\mu^f l_1^2 \mathbf{I}_{3\times3}\boldsymbol{\chi}_b;\ \mathbf{m}_s^f = 2\mu^f l_1^2 \mathbf{I}_{2\times2}\boldsymbol{\chi}_s \\ \mathbf{p}^f = 2\mu^f l_2^2 \mathbf{I}_{3\times3}\boldsymbol{\zeta} \\ \boldsymbol{\tau}_b^f = 2\mu^f l_3^2 \mathbf{I}_{6\times6}\boldsymbol{\eta}_b;\ \boldsymbol{\tau}_s^f = 2\mu^f l_3^2 \mathbf{I}_{4\times4}\boldsymbol{\eta}_s \end{cases} \tag{19}$$

where

$$\begin{aligned} &\boldsymbol{\sigma}_s^f = \{\tau_{xz} \quad \tau_{yz}\}^T;\ \boldsymbol{\sigma}_b^f = \{\sigma_x \quad \sigma_y \quad \tau_{x\nu}\}^T; \\ &\mathbf{B}_s = \left\{B_x^f \quad B_y^f\right\}^T;\ \mathbf{B}_b = \{0 \quad 0 \quad B_z\}^T; \\ &\mathbf{D}_s = \left\{D_x^f \quad D_y^f\right\}^T;\ \mathbf{D}_b = \left\{0 \quad 0 \quad D_z\right\}^T; \\ &\mathbf{H}_s = \{H_x \quad H_y\}^T;\ \mathbf{H}_b = \left\{0 \quad 0 \quad H_z\right\}^T; \\ &\mathbf{E}_s = \{E_x \quad E_y\}^T;\ \mathbf{E}_b = \{0 \quad 0 \quad E_z\}^T; \\ &\mathbf{m}_b^f = \left\{m_{xx}^f \quad m_{yy}^f \quad m_{xy}^f\right\}^T;\ \mathbf{m}_s^f = \left\{m_{xz}^f \quad m_{yz}^f\right\}^T; \\ &\mathbf{p}^f = \left\{p_x^f \quad p_y^f \quad p_z^f\right\}^T; \\ &\boldsymbol{\tau}_b^f = \left\{\tau_{xxx}^f \quad \tau_{yy}^f \quad \tau_{yyx}^f \quad \tau_{xy}^f \quad \tau_{zx}^f \quad \tau_{zy}^f\right\}^T; \\ &\boldsymbol{\tau}_s^f = \left\{\tau_{zz}^f \quad \tau_{xzz}^f \quad \tau_{yz}^f \quad \tau_{xyz}^f\right\}^T;\ \mu^f = \overline{c}_{66} \\ &\mathbf{C}_{bf} = \begin{bmatrix} \overline{c}_{11} & \overline{c}_{12} & 0 \\ \overline{c}_{12} & \overline{c}_{22} & 0 \\ 0 & 0 & \overline{c}_{66} \end{bmatrix};\ \mathbf{C}_{sf} = \begin{bmatrix} \overline{c}_{44} & 0 \\ 0 & \overline{c}_{55} \end{bmatrix}; \\ &\mathbf{C}_{ueb} = \begin{bmatrix} 0 & 0 & \overline{e}_{31} \\ 0 & 0 & \overline{e}_{31} \\ 0 & 0 & 0 \end{bmatrix};\ \mathbf{C}_{nmb} = \begin{bmatrix} 0 & 0 & \overline{q}_{31} \\ 0 & 0 & \overline{q}_{31} \\ 0 & 0 & 0 \end{bmatrix}; \\ &\mathbf{C}_{um\tau} = \begin{bmatrix} \overline{q}_{15} & 0 \\ 0 & \overline{q}_{15} \end{bmatrix};\ \mathbf{C}_{ues} = \begin{bmatrix} \overline{e}_{15} & 0 \\ 0 & \overline{e}_{15} \end{bmatrix}; \\ &\mathbf{C}_{esb} = \begin{bmatrix} 0 & 0 & 0 \\ 0 & 0 & 0 \\ 0 & 0 & \overline{k}_{33} \end{bmatrix};\ \mathbf{C}_{mmb} = \begin{bmatrix} 0 & 0 & 0 \\ 0 & 0 & 0 \\ 0 & 0 & \overline{\mu}_{33} \end{bmatrix}; \\ &\mathbf{C}_{esc} = \begin{bmatrix} \overline{k}_{11} & 0 \\ 0 & \overline{k}_{11} \end{bmatrix};\ \mathbf{C}_{mm} = \begin{bmatrix} \overline{\mu}_{11} & 0 \\ 0 & \overline{\mu}_{22} \end{bmatrix}; \\ &\mathbf{C}_{emb} = \begin{bmatrix} 0 & 0 & 0 \\ 0 & 0 & 0 \\ 0 & 0 & \overline{d}_{33} \end{bmatrix};\ \mathbf{C}_{emc} = \begin{bmatrix} \overline{d}_{11} & 0 \\ 0 & \overline{d}_{22} \end{bmatrix} \end{aligned} \tag{20}$$

In Eq. 20, τ_{xxx}^f,τ_{yyy}^f,τ_{yyx}^f,τ_{xxy}^f,τ_{zzx}^f,τ_{zzy}^f, τ_{zzz}^f,τ_{xxz}^f,τ_{yyz}^f,τ_{yyz}^f, p_x^f,p_y^f,p_z^f, and m_{xx}^f,m_{yy}^f, m_{xy}^f,m_{xz}^f,m_{yz}^f denote the higher-order

stress components of the face sheets; $\sigma_x^f, \sigma_y^f, \tau_{xy}^f, \tau_{xz}^f, \tau_{yz}^f$, D_x, D_y, D_z and B_x, B_y, B_z respectively denote the stress components, electric and magnetic displacements; $\bar{e}_{ij}, \bar{q}_{ij}$, and $\bar{c}_{ij}$ respectively stand for the reduced piezoelectric, piezomagnetic and elastic coefficients; $\bar{k}_{ij}, \bar{\mu}_{ij}$, and $\bar{d}_{ij}$ are the reduced dielectric permittivity, electromagnetic permittivity, magnetic permittivity coefficients, respectively. The material parameters, which are diminished in Eq. 20, are computed by the following process

$$
\begin{aligned}
&\bar{c}_{11} = c_{11} - \frac{c_{13}^2}{c_{33}};\ \bar{c}_{12} = c_{12} - \frac{c_{13}^2}{c_{33}};\ \bar{c}_{66} = c_{66};\ \bar{c}_{55} = c_{55};\\
&\bar{c}_{44} = c_{44}; \bar{e}_{31} = e_{31} - \frac{e_{33}c_{13}}{c_{33}};\ \bar{e}_{15} = e_{15};\ \bar{q}_{15} = q_{15};\\
&\bar{q}_{31} = q_{31} - \frac{q_{33}c_{13}}{c_{33}};\ \bar{k}_{11} = k_{11};\ \bar{k}_{33} = k_{33} + \frac{e_{33}^2}{c_{33}};\\
&\bar{d}_{11} = d_{11};\ \bar{d}_{33} = d_{33} + \frac{q_{33}e_{33}}{c_{33}};\\
&\bar{\mu}_{11} = \mu_{11}; \bar{\mu}_{33} = \mu_{33} + \frac{q_{33}^2}{c_{33}}
\end{aligned}
\tag{21}
$$

where $c_{ij}, q_{ij}, e_{ij}, \mu_{ij}$ and k_{ij} represent the material parameters as outlined in Table 3.

2.4. The Hamilton principle

Formulated according to Hamilton's principle, the MEE sandwich microplate's governing equation can be defined as by

$$
\int_0^t \left(\delta\Pi + \delta K - \delta V\right) \mathrm{d}t = 0 \tag{22}
$$

Here, δK, $\delta\Pi$ and δV are respectively represent the virtual kinetic energy, strain energy, and the work done by the electric and magnetic potentials.

The definition of the virtual strain energy for the microplate using MSGT [1] is provided in

$$
\begin{aligned}
\delta\Pi = &\int_\Omega \delta\bar{\boldsymbol{\varepsilon}}_b^T \bar{D}_b \bar{\boldsymbol{\varepsilon}}_b \mathrm{d}\Omega - \int_\Omega \delta\bar{\boldsymbol{\varepsilon}}_b^T \bar{D}_{ueb} \bar{\mathbf{E}}_b \mathrm{d}\Omega\\
&- \int_\Omega \delta\bar{\boldsymbol{\varepsilon}}_b^T \bar{D}_{umb} \bar{\mathbf{H}}_b \mathrm{d}\Omega + \int_\Omega \delta\boldsymbol{\varepsilon}_s^T \bar{D}_s \boldsymbol{\varepsilon}_s^T \mathrm{d}\Omega\\
&- \int_\Omega \delta\boldsymbol{\varepsilon}_s^T \bar{D}_{ues} \bar{\mathbf{E}}_s \mathrm{d}\Omega - \int_\Omega \delta\boldsymbol{\varepsilon}_s^T \bar{D}_{ums} \bar{\mathbf{H}}_s \mathrm{d}\Omega\\
&- \int_\Omega \delta\bar{\mathbf{E}}_b^T \bar{D}_{ueb}^T \bar{\boldsymbol{\varepsilon}}_b \mathrm{d}\Omega - \int_\Omega \delta\bar{\mathbf{E}}_b^T \bar{D}_{eeb} \bar{\mathbf{E}}_b \mathrm{d}\Omega\\
&- \int_\Omega \delta\bar{\mathbf{E}}_b^T \bar{D}_{emb} \bar{\mathbf{H}}_b \mathrm{d}\Omega - \int_\Omega \delta\bar{\mathbf{E}}_s^T \bar{D}_{ues}^T \boldsymbol{\varepsilon}_s \mathrm{d}\Omega\\
&- \int_\Omega \delta\bar{\mathbf{E}}_s^T \bar{D}_{ees} \bar{\mathbf{E}}_s \mathrm{d}\Omega - \int_\Omega \delta\bar{\mathbf{E}}_s^T \bar{D}_{ems} \bar{\mathbf{H}}_s \mathrm{d}\Omega\\
&- \int_\Omega \delta\bar{\mathbf{H}}_b^T \bar{D}_{umb}^T \bar{\boldsymbol{\varepsilon}}_b \mathrm{d}\Omega - \int_\Omega \delta\bar{\mathbf{H}}_b^T \bar{D}_{emb} \bar{\mathbf{E}}_b \mathrm{d}\Omega\\
&- \int_\Omega \delta\bar{\mathbf{H}}_b^T \bar{D}_{mmb} \bar{\mathbf{H}}_b \mathrm{d}\Omega - \int_\Omega \delta\bar{\mathbf{H}}_s^T \bar{D}_{ums}^T \boldsymbol{\varepsilon}_s \mathrm{d}\Omega\\
&- \int_\Omega \delta\bar{\mathbf{H}}_s^T \bar{D}_{ems} \bar{\mathbf{E}}_s \mathrm{d}\Omega - \int_\Omega \delta\bar{\mathbf{H}}_s^T \bar{D}_{mms} \bar{\mathbf{H}}_s \mathrm{d}\Omega\\
&+ \int_\Omega \delta\bar{\boldsymbol{\chi}}_b^T \bar{D}_{rb} \bar{\boldsymbol{\Gamma}}_{rb} \bar{\boldsymbol{\chi}}_b \mathrm{d}\Omega + \int_\Omega \delta\boldsymbol{\chi}_s^T \bar{D}_{rs} \bar{\boldsymbol{\Gamma}}_{rs} \boldsymbol{\chi}_s \mathrm{d}\Omega\\
&+ \int_\Omega \delta\bar{\boldsymbol{\zeta}}^T \bar{D}_{dil} \bar{\boldsymbol{\zeta}} \mathrm{d}\Omega + \int_\Omega \delta\bar{\boldsymbol{\eta}}_b^T \bar{D}_{deb} \bar{\boldsymbol{\Gamma}}_{deb} \bar{\boldsymbol{\eta}}_b \mathrm{d}\Omega\\
&+ \int_\Omega \delta\bar{\boldsymbol{\eta}}_s^T \bar{D}_{des} \bar{\boldsymbol{\Gamma}}_{des} \bar{\boldsymbol{\eta}}_s \mathrm{d}\Omega
\end{aligned}
\tag{23}
$$

where

$$
\bar{\boldsymbol{\varepsilon}}_b = \begin{Bmatrix} \varepsilon_1 \\ \varepsilon_2 \end{Bmatrix}; \bar{\mathbf{H}}_b = -\begin{Bmatrix} 0 \\ 0 \\ \psi \end{Bmatrix}; \bar{\mathbf{E}}_b = -\begin{Bmatrix} 0 \\ 0 \\ \varphi \end{Bmatrix}; \bar{\mathbf{H}}_s = -\begin{Bmatrix} \psi_{,x} \\ \psi_{,y} \end{Bmatrix};
$$

$$
\bar{\mathbf{E}}_s = -\begin{pmatrix} \varphi_{,x} \\ \varphi_{,y} \end{pmatrix}; \bar{\mathbf{D}}_b = \begin{bmatrix} \mathbf{A}^b & \mathbf{B}^b \\ \mathbf{B}^b & \mathbf{D}^b \end{bmatrix};
$$

$$
\bar{\mathbf{D}}_{ueb} = \begin{Bmatrix} \mathbf{C}_{ueb}^1 & \mathbf{C}_{ueb}^2 \end{Bmatrix}; \bar{D}_{umb} = \begin{Bmatrix} \mathbf{C}_{umb}^1 & \mathbf{C}_{umb}^2 \end{Bmatrix};
$$

$$
\left(\mathbf{A^b}, \mathbf{B^b}, \mathbf{D^b}\right) = \int_{-h_c/2}^{h_c/2} \left(z^2, zf, f^2\right) \mathbf{C}_{bc} \mathrm{d}z
$$

$$
+ \int_{-h/2}^{-h_c/2} \left(z^2, zf, f^2\right) \mathbf{C}_{bf} \mathrm{d}z + \int_{h_c/2}^{h/2} \left(z^2, zf, f^2\right) \mathbf{C}_{bf} \mathrm{d}z;
$$

$$
\bar{\mathbf{D}}_{\mathbf{s}} = \int_{-h_c/2}^{h_c/2} (1+f')^2 \mathbf{C}_{sc} \mathrm{d}z + \int_{-h/2}^{-h_c/2} (1+f')^2 \mathbf{C}_{sf} \mathrm{d}z
$$

$$
+ \int_{h_c/2}^{h/2} (1+f')^2 \mathbf{C}_{sf} \mathrm{d}z;
$$

$$
\left(\mathbf{C}_{ueb}^1, \mathbf{C}_{ueb}^2\right) = \int_{-h/2}^{-h_c/2} g'(z,f) \mathbf{C}_{ueb} \mathrm{d}z + \int_{h_c/2}^{h/2} g'(z,f) \mathbf{C}_{ueb} \mathrm{d}z;
$$

$$
\left(\mathbf{C}_{umb}^1, \mathbf{C}_{umb}^2\right) = \int_{-h/2}^{-h_c/2} g'(z,f) \mathbf{C}_{umb} \mathrm{d}z + \int_{h_c/2}^{h/2} g'(z,f) \mathbf{C}_{umb} \mathrm{d}z;
$$

$$\bar{\mathbf{D}}_{ues}=\int_{-h/2}^{-h_c/2} g\left(1+f'\right)\mathbf{C}_{ues}\mathrm{d}z+\int_{h_c/2}^{h/2} g\left(1+f'\right)\mathbf{C}_{ues}\mathrm{d}z;$$
$$\bar{\mathbf{D}}_{ums}=\int_{-h/2}^{-h_c/2} g\left(1+f'\right)\mathbf{C}_{ums}\mathrm{d}z+\int_{h_c/2}^{h/2} g\left(1+f'\right)\mathbf{C}_{ums}\mathrm{d}z;$$
$$\bar{\mathbf{D}}_{emb}=\int_{-h/2}^{-h_c/2} g'^2\mathbf{C}_{emb}\mathrm{d}z+\int_{h_c/2}^{h/2} g'^2\mathbf{C}_{emb}\mathrm{d}z;$$
$$\bar{\mathbf{D}}_{eeb}=\int_{-h/2}^{-h_c/2} g'^2\mathbf{C}_{eeb}\mathrm{d}z+\int_{h_c/2}^{h/2} g'^2\mathbf{C}_{eeb}\mathrm{d}z;$$
$$\bar{\mathbf{D}}_{mmb}=\int_{-h/2}^{-h_c/2} g'^2\mathbf{C}_{mmb}\mathrm{d}z+\int_{h_c/2}^{h/2} g'^2\mathbf{C}_{mmb}\mathrm{d}z;$$
$$\bar{\mathbf{D}}_{mms}=\int_{-h/2}^{-h_c/2} g^2\mathbf{C}_{mms}\mathrm{d}z+\int_{h_c/2}^{h/2} g^2\mathbf{C}_{mms}\mathrm{d}z;$$
$$\bar{\mathbf{D}}_{ees}=\int_{-h/2}^{-h_c/2} g^2\mathbf{C}_{ees}\mathrm{d}z+\int_{h_c/2}^{h/2} g^2\mathbf{C}_{ees}\mathrm{d}z;$$
$$\bar{\mathbf{D}}_{ems}=\int_{-h/2}^{-h_c/2} g^2\mathbf{C}_{ems}\mathrm{d}z+\int_{h_c/2}^{h/2} g^2\mathbf{C}_{ems}\mathrm{d}z \tag{24}$$

and

$$\bar{\mathbf{D}}_{ub}=\begin{bmatrix}\mathbf{A}_b & \mathbf{B}_b\\ \mathbf{B}_b & \mathbf{D}_b\end{bmatrix};\ \bar{\mathbf{D}}_{rb}=\begin{bmatrix}\mathbf{A}_{rb} & \mathbf{B}_{rb}\\ \mathbf{B}_{rb} & \mathbf{D}_{rb}\end{bmatrix};$$
$$\left(\mathbf{A}_b,\mathbf{B}_b,\mathbf{D}_b\right)=\int_{-h/2}^{h/2}\left(z^2,zf,f^2\right)\mathbf{C}_{ub}\mathrm{d}z;$$
$$\left(\mathbf{A}_{rb},\mathbf{B}_{rb},\mathbf{D}_{rb}\right)=\int_{-h/2}^{h/2} 2\mu {l_1}^2\left(1,f',f'^2\right)I_{3x3}\mathrm{d}z;$$
$$\left(\mathbf{A}_{rs},\mathbf{B}_{rs},\mathbf{D}_{rs}\right)=\int_{-h/2}^{h/2} 2\mu {l_1}^2\left(1,f",f"^2\right)I_{2x2}\mathrm{d}z$$
$$\bar{\mathbf{D}}_{di}=\begin{bmatrix}\mathbf{A}_{di} & \mathbf{B}_{di} & \mathbf{C}_{di} & \mathbf{E}_{di}\\ \mathbf{B}_{di} & \mathbf{D}_{di} & \mathbf{F}_{di} & \mathbf{L}_{di}\\ \mathbf{C}_{di} & \mathbf{F}_{di} & \mathbf{H}_{di} & \mathbf{O}_{di}\\ \mathbf{E}_{di} & \mathbf{L}_{di} & \mathbf{O}_{di} & \mathbf{P}_{di}\end{bmatrix};$$
$$\bar{\mathbf{D}}_{dsb}=\begin{bmatrix}\mathbf{A}_{dsb} & \mathbf{B}_{dsb} & \mathbf{C}_{dsb} & \mathbf{E}_{dsb}\\ \mathbf{B}_{dsb} & \mathbf{D}_{dsb} & \mathbf{F}_{dsb} & \mathbf{L}_{dsb}\\ \mathbf{C}_{dsb} & \mathbf{F}_{dsb} & \mathbf{H}_{dsb} & \mathbf{O}_{dsb}\\ \mathbf{E}_{dsb} & \mathbf{L}_{dsb} & \mathbf{O}_{dsb} & \mathbf{P}_{dsb}\end{bmatrix};$$
$$\mathbf{A}_{di},\mathbf{B}_{di},\mathbf{D}_{di},\mathbf{C}_{di},\mathbf{E}_{di},\mathbf{F}_{di},\mathbf{L}_{di},\mathbf{H}_{di},\mathbf{O}_{di},\mathbf{P}_{di})=$$
$$\int_{-h/2}^{h/2} 2\mu l_2^2\left(1,z,z^2,f,f',zf,zf',f^2,ff',f'^2\right)\mathbf{I}_{3x3}\mathrm{d}z;$$
$$\mathbf{A}_{deb},\mathbf{B}_{deb},\mathbf{D}_{deb},\mathbf{C}_{deb},\mathbf{E}_{deb},\mathbf{F}_{deb},\mathbf{L}_{deb},\mathbf{H}_{deb},\mathbf{O}_{deb},\mathbf{P}_{deb})=$$
$$\int_{-h/2}^{h/2} 2\mu l_3^2\left(1,z,z^2,f,f'',zf,zf'',f^2(z),ff'',f''^2\right)\mathbf{I}_{6x6}\mathrm{d}z;$$
$$\left(\mathbf{A}_{des},\mathbf{B}_{des},\mathbf{D}_{des}\right)=\int_{-h/2}^{h/2} 2\mu l_3^2\left(1,f',f'^2\right)\mathbf{I}_{4x4}\mathrm{d}z;$$
$$\bar{\mathbf{D}}_{rs}=\begin{bmatrix}\mathbf{A}_{rs} & \mathbf{B}_{rs}\\ \mathbf{B}_{rs} & \mathbf{D}_{rs}\end{bmatrix};\bar{\mathbf{D}}_{des}=\begin{bmatrix}\mathbf{A}_{des} & \mathbf{B}_{des}\\ \mathbf{B}_{des} & \mathbf{D}_{des}\end{bmatrix};$$
$$\overline{\mathbf{\Gamma}}_{deb}=\begin{bmatrix}\mathbf{\Gamma}_{deb} & \mathbf{0} & \mathbf{0} & \mathbf{0}\\ \mathbf{0} & \mathbf{\Gamma}_{deb} & \mathbf{0} & \mathbf{0}\\ \mathbf{0} & \mathbf{0} & \mathbf{\Gamma}_{deb} & \mathbf{0}\\ \mathbf{0} & \mathbf{0} & \mathbf{0} & \mathbf{\Gamma}_{deb}\end{bmatrix};$$
$$\overline{\mathbf{\Gamma}}_{rb}=\begin{bmatrix}\mathbf{\Gamma}_{rb} & \mathbf{0}\\ \mathbf{0} & \mathbf{\Gamma}_{rb}\end{bmatrix};\overline{\mathbf{\Gamma}}_{rs}=\begin{bmatrix}\mathbf{\Gamma}_{rs} & \mathbf{0}\\ \mathbf{0} & \mathbf{\Gamma}_{rs}\end{bmatrix};$$
$$\overline{\mathbf{\Gamma}}_{des}=\begin{bmatrix}\mathbf{\Gamma}_{des} & \mathbf{0}\\ \mathbf{0} & \mathbf{\Gamma}_{des}\end{bmatrix};$$
$$\mathbf{\Gamma}_{rb}=diag\left(1,1,2\right);\mathbf{\Gamma}_{rs}=diag\left(2,2\right);$$
$$\mathbf{\Gamma}_{des}=diag(1,3,3,6);\mathbf{\Gamma}_{deb}=diag(1,1,3,3,3,3) \tag{25}$$

The expression for the virtual kinetic energy is given as follows

$$\delta K=\int_{\Omega}\delta\bar{\mathbf{u}}^T\bar{\mathbf{m}}\ddot{\bar{\mathbf{u}}}\mathrm{d}\Omega \tag{26}$$

where

$$\bar{\mathbf{u}}=\begin{cases}\mathbf{u}_1\\ \mathbf{u}_2\\ \mathbf{u}_3\end{cases};\bar{\mathbf{m}}=\begin{bmatrix}\mathbf{I}_0 & \mathbf{0} & \mathbf{0}\\ \mathbf{0} & \mathbf{I}_0 & \mathbf{0}\\ \mathbf{0} & \mathbf{0} & \mathbf{I}_0\end{bmatrix};\mathbf{I}_0=\begin{bmatrix}I_1 & I_2 & I_4\\ I_2 & I_3 & I_5\\ I_4 & I_5 & I_6\end{bmatrix}$$
$$\left(I_1,I_2,I_3,I_4,I_5,I_6\right)=\int_{-h/2}^{h/2}\left(1,z,z^2,f,zf,f^2\right)\rho\left(z\right)\mathrm{d}z \tag{27}$$

Moreover, the virtual work is accounted for by

$$\delta V=\int_{\Omega}\delta\mathbf{N}_w^T\mathbf{N}^{em}\mathbf{N}_w\mathrm{d}\Omega \tag{28}$$

in which

$$\mathbf{N}_w=\begin{Bmatrix}w_{b,x}+w_{s,x}\\ w_{b,y}+w_{s,y}\end{Bmatrix};$$
$$\mathbf{N}^{em}=-\begin{bmatrix}2\left(\bar{e}_{31}\phi_0+\bar{q}_{31}\psi_0\right) & 0\\ 0 & 2\left(\bar{e}_{31}\phi_0+\bar{q}_{31}\psi_0\right)\end{bmatrix} \tag{29}$$

By incorporating the required expressions into Eq. 22, the weak form of the microplates is revised as follow

$$\int_{\Omega}\delta\bar{\boldsymbol{\varepsilon}}_b^T\bar{D}_b\bar{\boldsymbol{\varepsilon}}_b\mathrm{d}\Omega-\int_{\Omega}\delta\bar{\boldsymbol{\varepsilon}}_b^T\bar{D}_{ueb}\bar{\mathbf{E}}_b\mathrm{d}\Omega$$
$$-\int_{\Omega}\delta\bar{\boldsymbol{\varepsilon}}_b^T\bar{D}_{umb}\bar{\mathbf{H}}_b\mathrm{d}\Omega+\int_{\Omega}\delta\boldsymbol{\varepsilon}_s^T\bar{D}_s\boldsymbol{\varepsilon}_s^T\mathrm{d}\Omega$$
$$-\int_{\Omega}\delta\boldsymbol{\varepsilon}_s^T\bar{D}_{ues}\bar{\mathbf{E}}_s\mathrm{d}\Omega-\int_{\Omega}\delta\boldsymbol{\varepsilon}_s^T\bar{D}_{ums}\bar{\mathbf{H}}_s\mathrm{d}\Omega$$
$$-\int_{\Omega}\delta\bar{\mathbf{E}}_b^T\bar{D}_{ueb}^T\bar{\boldsymbol{\varepsilon}}_b\mathrm{d}\Omega-\int_{\Omega}\delta\bar{\mathbf{E}}_b^T\bar{D}_{eeb}\bar{\mathbf{E}}_b\mathrm{d}\Omega$$
$$\int_{\Omega}\delta\bar{\boldsymbol{\varepsilon}}_b^T\bar{D}_b\bar{\boldsymbol{\varepsilon}}_b\mathrm{d}\Omega-\int_{\Omega}\delta\bar{\boldsymbol{\varepsilon}}_b^T\bar{D}_{ueb}\bar{\mathbf{E}}_b\mathrm{d}\Omega$$
$$-\int_{\Omega}\delta\bar{\boldsymbol{\varepsilon}}_b^T\bar{D}_{umb}\bar{\mathbf{H}}_b\mathrm{d}\Omega+\int_{\Omega}\delta\boldsymbol{\varepsilon}_s^T\bar{D}_s\boldsymbol{\varepsilon}_s^T\mathrm{d}\Omega$$
$$-\int_{\Omega}\delta\boldsymbol{\varepsilon}_s^T\bar{D}_{ues}\bar{\mathbf{E}}_s\mathrm{d}\Omega-\int_{\Omega}\delta\boldsymbol{\varepsilon}_s^T\bar{D}_{ums}\bar{\mathbf{H}}_s\mathrm{d}\Omega$$
$$-\int_{\Omega}\delta\bar{\mathbf{E}}_b^T\bar{D}_{ueb}^T\bar{\boldsymbol{\varepsilon}}_b\mathrm{d}\Omega-\int_{\Omega}\delta\bar{\mathbf{E}}_b^T\bar{D}_{eeb}\bar{\mathbf{E}}_b\mathrm{d}\Omega$$

$$
\begin{aligned}
&-\int_{\Omega}\delta\bar{\mathbf{E}}_b^T\bar{D}_{emb}\bar{\mathbf{H}}_b\mathrm{d}\Omega-\int_{\Omega}\delta\bar{\mathbf{E}}_s^T\bar{D}_{ues}^T\boldsymbol{\varepsilon}_s\mathrm{d}\Omega\\
&-\int_{\Omega}\delta\bar{\mathbf{E}}_s^T\bar{D}_{ees}\bar{\mathbf{E}}_s\mathrm{d}\Omega-\int_{\Omega}\delta\bar{\mathbf{E}}_s^T\bar{D}_{ems}\bar{\mathbf{H}}_s\mathrm{d}\Omega\\
&-\int_{\Omega}\delta\bar{\mathbf{H}}_b^T\bar{D}_{umb}^T\bar{\boldsymbol{\varepsilon}}_b\mathrm{d}\Omega-\int_{\Omega}\delta\bar{\mathbf{H}}_b^T\bar{D}_{emb}\bar{\mathbf{E}}_b\mathrm{d}\Omega\\
&-\int_{\Omega}\delta\bar{\mathbf{H}}_b^T\bar{D}_{mmb}\bar{\mathbf{H}}_b\mathrm{d}\Omega-\int_{\Omega}\delta\bar{\mathbf{H}}_s^T\bar{D}_{ums}^T\boldsymbol{\varepsilon}_s\mathrm{d}\Omega\\
&-\int_{\Omega}\delta\bar{\mathbf{H}}_s^T\bar{D}_{ems}\bar{\mathbf{E}}_s\mathrm{d}\Omega-\int_{\Omega}\delta\bar{\mathbf{H}}_s^T\bar{D}_{mms}\bar{\mathbf{H}}_s\mathrm{d}\Omega\\
&+\int_{\Omega}\delta\bar{\boldsymbol{\chi}}_b^T\bar{D}_{rb}\bar{\boldsymbol{\Gamma}}_{rb}\bar{\boldsymbol{\chi}}_b\mathrm{d}\Omega+\int_{\Omega}\delta\boldsymbol{\chi}_s^T\bar{D}_{rs}\bar{\boldsymbol{\Gamma}}_{rs}\boldsymbol{\chi}_s\mathrm{d}\Omega\\
&+\int_{\Omega}\delta\bar{\boldsymbol{\zeta}}^T\bar{D}_{dil}\bar{\boldsymbol{\zeta}}\mathrm{d}\Omega+\int_{\Omega}\delta\bar{\boldsymbol{\eta}}_b^T\bar{D}_{deb}\bar{\boldsymbol{\Gamma}}_{deb}\bar{\boldsymbol{\eta}}_b\mathrm{d}\Omega\\
&+\int_{\Omega}\delta\bar{\boldsymbol{\eta}}_s^T\bar{D}_{des}\bar{\boldsymbol{\Gamma}}_{des}\bar{\boldsymbol{\eta}}_s\mathrm{d}\Omega+\int_{\Omega}\delta\bar{\mathbf{u}}^T\bar{\mathbf{m}}\ddot{\bar{\mathbf{u}}}\mathrm{d}\Omega\\
&-\int_{\Omega}\delta\mathbf{N}_w^T\mathbf{N}^{em}\mathbf{N}_w\mathrm{d}\Omega=\mathbf{0}
\end{aligned}
\tag{30}
$$

3. The NURBS formulation

In two dimensions (2D), Non-Uniform Rational B-Splines (NURBS) basis functions [21] are constructed using two knot vector and . In this context, $\boldsymbol{\Theta}=\{\eta_1,\eta_2,\ldots,\eta_{n+p+1}\}$ and $\mathrm{H}=\{\zeta_1,\zeta_2,\ldots,\zeta_{m+q+1}\}$ represent the number of control points, while p and q denote the polynomial orders. The knot vectors are denoted by $\boldsymbol{\Theta}$ and H .The computation of the basis functions for two-dimensional B-splines involves:

$$
R_{i,j}(\eta,\zeta)=\tilde{N}_{i,p}(\eta)\,\tilde{M}_{j,q}(\zeta) \tag{31}
$$

The B-spline basic functions $\tilde{N}$ and $\tilde{M}$ are constructed using the Cox-de Boor algorithm, as described below

$$
\begin{aligned}
\tilde{M}_{j,0}(\zeta)&=\begin{cases}1 & \text{if } \zeta_j\le\zeta\le\zeta_{j+1}\\ 0 & \text{otherwise}\end{cases} && (q=0)\\
\tilde{N}_{i,0}(\eta)&=\begin{cases}1 & \text{if } \eta_i\le\eta\le\eta_{i+1}\\ 0 & \text{otherwise}\end{cases} && (p=0)
\end{aligned}
\tag{32}
$$

and

$$
\begin{aligned}
\tilde{M}_{j,q}(\zeta)&=\frac{\zeta-\zeta_j}{\zeta_{j+q}-\zeta_j}\tilde{M}_{j,q-1}(\zeta)\\
&\quad+\frac{\zeta_{j+q+1}-\zeta}{\zeta_{j+q+1}-\zeta_{j+1}}\tilde{M}_{j+1,q-1}(\zeta)\quad(q\ge1);\\
\tilde{N}_{i,p}(\eta)&=\frac{\eta-\eta_i}{\eta_{i+p}-\eta_i}\tilde{N}_{i,p-1}(\eta)\\
&\quad+\frac{\eta_{i+p+1}-\eta}{\eta_{i+p+1}-\eta_{i+1}}\tilde{N}_{i+1,p-1}(\eta)\qquad(p\ge1)
\end{aligned}
\tag{33}
$$

NURBS basic functions are formulated by combining B-spline basic functions with their corresponding weights, as shown below

$$
N_{i,j}(\eta,\zeta)=N_e(\breve{})=\frac{\tilde{N}_{i,p}(\eta)\,\tilde{M}_{j,q}(\zeta)\,w_{i,j}}{\sum_{\hat{i}=1}^{n}\sum_{\hat{j}=1}^{m}\tilde{N}_{i,p}(\eta)\,\tilde{M}_{\hat{j},q}(\zeta)\,w_{\hat{i},\hat{j}}} \tag{34}
$$

The approximation of the displacement vector, magnetic and electric fields based on the NURBS basic function is expressed by following

$$
\begin{aligned}
\mathbf{u}(x,y)&=\sum_{I=1}^{m\times n}\mathbf{N}_I(x,y)\,\mathbf{q}_I;\\
\psi(x,y)&=\sum_{I=1}^{m\times n}\mathbf{N}_{\psi I}(x,y)\,\boldsymbol{\chi}_I;\\
\varphi(x,y)&=\sum_{I=1}^{m\times n}\mathbf{N}_{\varphi I}(x,y)\,\chi_I
\end{aligned}
\tag{35}
$$

where

$$
\begin{aligned}
&\mathbf{N}_I(x,y)=N_I(x,y)\,\mathbf{I}_{2\times2};\mathbf{q}_I=\begin{Bmatrix}w_{bI} & w_{sI}\end{Bmatrix}^T;\\
&\mathbf{N}_{\varphi I}(x,y)=\begin{Bmatrix}N_I(x,y) & 0\end{Bmatrix};\\
&\mathbf{N}_{\psi I}(x,y)=\begin{Bmatrix}0 & N_I(x,y)\end{Bmatrix};\\
&\chi_I=\begin{Bmatrix}\varphi_I & \psi_I\end{Bmatrix}^T
\end{aligned}
\tag{36}
$$

where the NURBS basic function is denoted by $N_I(x,y)$.

Based on the approximation 35, the displacement $\bar{\mathbf{u}}$ is reformed as follow

$$
\bar{\mathbf{u}}=\begin{Bmatrix}\mathbf{u}_1\\ \mathbf{u}_2\\ \mathbf{u}_3\end{Bmatrix}=\sum_{I=1}^{m\times n}\begin{Bmatrix}\mathbf{N}_{1I}\\ \mathbf{N}_{2I}\\ \mathbf{N}_{3I}\end{Bmatrix}\mathbf{q}_I=\sum_{I=1}^{m\times n}\bar{\mathbf{N}}_{uI}\mathbf{q}_I \tag{37}
$$

where

$$\mathbf{N}_{1I}=\begin{bmatrix}0 & 0\\ 0 & 0\\ N_I & N_I\end{bmatrix};\mathbf{N}_{2I}=\begin{bmatrix}-N_{I,x} & 0\\ -N_{I,y} & 0\\ 0 & 0\end{bmatrix};\quad \mathbf{N}_{3I}=\begin{bmatrix}0 & N_{I,x}\\ 0 & N_{I,y}\\ 0 & 0\end{bmatrix} \tag{38}$$

The strain tensor, rotation gradient, deviatoric stretch gradient, dilatation gradient and electric and magnetic fields are reformed according to the approximation in Eq. 35, as follows

$$\bar{\boldsymbol{\varepsilon}}_b=\left\{\begin{array}{c}\bar{\boldsymbol{\varepsilon}}_1\\ \bar{\boldsymbol{\varepsilon}}_2\end{array}\right\}=\sum_{I=1}^{m\times n}\left\{\begin{array}{c}\bar{\mathbf{B}}_{b1I}\\ \bar{\mathbf{B}}_{b2I}\end{array}\right\}\mathbf{q}_I=\sum_{I=1}^{m\times n}\bar{\mathbf{B}}_{bI}\mathbf{q}_I;$$

$$\bar{\boldsymbol{\varepsilon}}_s=\sum_{I=1}^{m\times n}\bar{\mathbf{B}}_{sI}\mathbf{d}_I;\ \boldsymbol{\chi}_s=\sum_{I=1}^{m\times n}\bar{\mathbf{B}}_{rsI}\mathbf{q}_I;$$

$$\bar{\boldsymbol{\chi}}^b=\left\{\begin{array}{c}\boldsymbol{\chi}_1^b\\ \boldsymbol{\chi}_2^b\end{array}\right\}=\sum_{I=1}^{m\times n}\left\{\begin{array}{c}\mathbf{B}_{rI}^{b1}\\ \mathbf{B}_{rI}^{b2}\end{array}\right\}\mathbf{q}_I=\sum_{I=1}^{m\times n}\bar{\mathbf{B}}_{rbI}\mathbf{q}_I;$$

$$\bar{\boldsymbol{\zeta}}=\sum_{I=1}^{m\times n}\left\{\begin{array}{c}\mathbf{B}_{1I}^{dil}\\ \mathbf{B}_{2I}^{dil}\\ \mathbf{B}_{3I}^{dil}\\ \mathbf{B}_{4I}^{dil}\end{array}\right\}\mathbf{q}_I=\sum_{I=1}^{m\times n}\bar{\mathbf{B}}_{dilI}\mathbf{q}_I;$$

$$\bar{\boldsymbol{\eta}}^b=\left\{\begin{array}{c}\bar{\boldsymbol{\eta}}_1^b\\ \bar{\boldsymbol{\eta}}_2^b\\ \bar{\boldsymbol{\eta}}_3^b\end{array}\right\}=\sum_{I=1}^{m\times n}\left\{\begin{array}{c}\mathbf{B}_{1I}^{deb}\\ \mathbf{B}_{2I}^{deb}\\ \mathbf{B}_{3I}^{deb}\end{array}\right\}\mathbf{q}_I=\sum_{I=1}^{m\times n}\bar{\mathbf{B}}_{debI}\mathbf{q}_I$$

$$\bar{\boldsymbol{\eta}}^s=\left\{\begin{array}{c}\bar{\boldsymbol{\eta}}_1^s\\ \bar{\boldsymbol{\eta}}_2^s\end{array}\right\}=\sum_{I=1}^{m\times n}\left\{\begin{array}{c}\mathbf{B}_{1I}^{des}\\ \mathbf{B}_{2I}^{des}\end{array}\right\}\mathbf{q}_I=\sum_{I=1}^{m\times n}\bar{\mathbf{B}}_{desI}\mathbf{q}_I$$

$$\bar{\mathbf{E}}_b=\sum_{I=1}^{m\times n}\bar{\mathbf{B}}_{ebI}\boldsymbol{\Lambda}_I;\bar{\mathbf{E}}_s=\sum_{I=1}^{m\times n}\bar{\mathbf{B}}_{esI}\boldsymbol{\Lambda}_I;$$

$$\bar{\mathbf{H}}_b=\sum_{I=1}^{m\times n}\bar{\mathbf{B}}_{mbI}\boldsymbol{\Lambda}_I;\bar{\mathbf{H}}_s=\sum_{I=1}^{m\times n}\bar{\mathbf{B}}_{msI}\boldsymbol{\Lambda}_I; \tag{39}$$

in which

$$\mathbf{B}_I^s=\begin{bmatrix}0 & N_{I,x}\\ 0 & N_{I,y}\end{bmatrix};\overline{\mathbf{B}}_{ebI}=\left\{\begin{array}{c}0\\ 0\\ -N_I\end{array}\right\};$$

$$\overline{\mathbf{B}}_{esI}=\left\{\begin{array}{c}-N_{I,x}\\ -N_{I,y}\end{array}\right\};\mathbf{B}_{rsI}=\frac{1}{4}\begin{bmatrix}0 & -N_{I,y}\\ 0 & N_{I,x}\end{bmatrix};$$

$$\mathbf{B}_{1I}^b=-\begin{bmatrix}N_{I,xx} & 0\\ N_{I,yy} & 0\\ 2N_{I,xy} & 0\end{bmatrix};\mathbf{B}_{2I}^b=\begin{bmatrix}0 & N_{I,xx}\\ 0 & N_{I,yy}\\ 0 & 2N_{I,xy}\end{bmatrix};$$

$$\mathbf{B}_{1I}^{deb}=\frac{1}{5}\begin{bmatrix}-2N_{I,xx}+3N_{I,xyy} & 0\\ -2N_{I,yyy}+3N_{I,xyy} & 0\\ N_{I,xxy}-4N_{I,xyy} & 0\\ N_{I,yy}-4N_{I,xyy} & 0\\ N_{I,xx}+N_{I,xyy} & 0\\ N_{I,yy}+N_{I,xy} & 0\end{bmatrix};$$

$$\mathbf{B}_{2I}^{deb}=\frac{1}{5}\begin{bmatrix}0 & 2N_{I,xx}-3N_{I,xyy}\\ 0 & 2N_{I,xyy}-3N_{I,xxy}\\ 0 & -N_{I,xxx}+4N_{I,xyy}\\ 0 & -N_{I,yyy}+4N_{I,xyy}\\ 0 & -N_{I,xxx}-N_{I,xyy}\\ 0 & -N_{I,yyy}-N_{I,xyy}\end{bmatrix};$$

$$\mathbf{B}_{3i}^{deb}=\frac{1}{15}\begin{bmatrix}0 & -3N_{I,x}\\ 0 & -3N_{I,y}\\ 0 & -N_{I,x}\\ 0 & -N_{I,y}\\ 0 & 4N_{I,x}\\ 0 & 4N_{I,y}\end{bmatrix};$$

$$\mathbf{B}_{1L}^{des}=\frac{1}{15}\begin{bmatrix}3N_{I,xx}+3N_{I,yy} & -3N_{I,xx}-3N_{I,yy}\\ -4N_{I,xx}+N_{I,yy} & 4N_{I,xx}-N_{I,yy}\\ -4N_{I,yy}+N_{I,xx} & 4N_{I,yy}-N_{I,xx}\\ -5N_{I,xy} & 5N_{I,xy}\end{bmatrix};$$

$$\mathbf{B}_{rI}^{b1}=\frac{1}{4}\begin{bmatrix}4N_{I,xy} & 2N_{I,xy}\\ -4N_{I,xy} & -2N_{I,xy}\\ 2\left(N_{I,yy}-N_{Ixx}\right) & N_{I,yy}-N_{I,xx}\end{bmatrix};$$

$$\mathbf{B}_{rI}^{b2}=\frac{1}{4}\begin{bmatrix}0 & -2N_{I,xy}\\ 0 & 2N_{I,xy}\\ 0 & N_{I,xx}-N_{I,yy}\end{bmatrix};$$

$$\mathbf{B}_{1I}^{dil}=-\begin{bmatrix}0 & 0\\ 0 & 0\\ N_{I,xx}+N_{I,yy} & 0\end{bmatrix};$$

$$\mathbf{B}_{2I}^{dil}=\begin{bmatrix}-N_{I,xxx}-N_{I,xyy} & 0\\ -N_{I,yy}-N_{I,xxy} & 0\\ 0 & 0\end{bmatrix};$$

$$\mathbf{B}_{3I}^{dil}=\begin{bmatrix}0 & N_{I,xxx}+N_{I,xyy}\\ 0 & N_{I,yyy}+N_{I,xxy}\\ 0 & 0\end{bmatrix};$$

$$\mathbf{B}_{4I}^{dil}=\begin{bmatrix}0 & 0\\ 0 & 0\\ 0 & N_{I,xx}+N_{I,yy}\end{bmatrix} \tag{40}$$

Similarly, the vector $\mathbf{N}_w$ is rewritten as follow

$$\mathbf{N}_w = \sum_{I=1}^{m\times n} \bar{\mathbf{B}}_{gI}\mathbf{q}_I; \bar{\mathbf{B}}_{gI} = \begin{bmatrix} N_{I,x} & N_{I,x} \\ N_{I,y} & N_{I,y} \end{bmatrix} \quad (41)$$

Substituting the necessary expressions into Eq. 30, the expression for the weak form in the free vibration analysis of the MEE sandwich microplate can be stated as follows

$$\left(\mathbf{K} - \omega^2\mathbf{M}\right)\bar{\mathbf{q}} = 0 \quad (42)$$

where

$$\begin{aligned}
\mathbf{K} &= \mathbf{K}_u - \mathbf{K}_{u\kappa}\mathbf{K}_{\kappa\kappa}^{-1}\mathbf{K}_{u\kappa}^T; \\
\mathbf{K}_{u\kappa} &= -\int_\Omega \bar{\mathbf{B}}_b^T \bar{D}_{ueb}\bar{\mathbf{B}}_{eb}\mathrm{d}\Omega - \int_\Omega \bar{\mathbf{B}}_b^T \bar{D}_{umb}\bar{\mathbf{B}}_{mb}\mathrm{d}\Omega \\
&\quad - \int_\Omega \bar{\mathbf{B}}_s^T \bar{D}_{ues}\bar{\mathbf{B}}_{es}\mathrm{d}\Omega - \int_\Omega \bar{\mathbf{B}}_s^T \bar{D}_{ums}\bar{\mathbf{B}}_{ms}\mathrm{d}\Omega; \\
\mathbf{K}_u &= \int_\Omega \bar{\mathbf{B}}_b^T \bar{D}_{ub}\bar{\mathbf{B}}_b\mathrm{d}\Omega + \int_\Omega \bar{\mathbf{B}}_s^T \bar{D}_{us}\bar{\mathbf{B}}_s\mathrm{d}\Omega \\
&\quad + \int_\Omega \bar{\mathbf{B}}_{rb}^T \bar{D}_{rb}\bar{\mathbf{\Gamma}}_{rb}\bar{\mathbf{B}}_{rb}\mathrm{d}\Omega + \int_\Omega \bar{\mathbf{B}}_{rs}^T \bar{D}_{rs}\bar{\mathbf{\Gamma}}_{rs}\bar{\mathbf{B}}_{rs}\mathrm{d}\Omega \\
&\quad + \int_\Omega \bar{\mathbf{B}}_{dil}^T \bar{D}_{dil}\bar{\mathbf{B}}_{dil}\mathrm{d}\Omega + \int_\Omega \bar{\mathbf{B}}_{deb}^T \bar{D}_{deb}\bar{\mathbf{\Gamma}}_{deb}\bar{\mathbf{B}}_{deb}\mathrm{d}\Omega \\
&\quad + \int_\Omega \bar{\mathbf{B}}_{des}^T \bar{D}_{des}\bar{\mathbf{\Gamma}}_{des}\bar{\mathbf{B}}_{des}\mathrm{d}\Omega - \int_\Omega \bar{\mathbf{B}}_g^T \mathbf{N}^{em}\bar{\mathbf{B}}_g\mathrm{d}\Omega; \\
\mathbf{K}_{\kappa\kappa} &= -\int_\Omega \bar{\mathbf{B}}_{eb}^T \bar{D}_{eeb}\bar{\mathbf{B}}_{eb}\mathrm{d}\Omega - \int_\Omega \bar{\mathbf{B}}_{eb}^T \bar{D}_{emb}\bar{\mathbf{B}}_{mb}\mathrm{d}\Omega \\
&\quad - \int_\Omega \bar{\mathbf{B}}_{es}^T \bar{D}_{ees}\bar{\mathbf{B}}_{es}\mathrm{d}\Omega - \int_\Omega \bar{\mathbf{B}}_{es}^T \bar{D}_{ems}\bar{\mathbf{B}}_{ms}\mathrm{d}\Omega \\
&\quad - \int_\Omega \bar{\mathbf{B}}_{mb}^T \bar{D}_{emb}\bar{\mathbf{B}}_{eb}\mathrm{d}\Omega - \int_\Omega \bar{\mathbf{B}}_{mb}^T \bar{D}_{mmb}\bar{\mathbf{B}}_{mb}\mathrm{d}\Omega \\
&\quad - \int_\Omega \bar{\mathbf{B}}_{ms}^T \bar{D}_{ems}\bar{\mathbf{B}}_{es}\mathrm{d}\Omega - \int_\Omega \bar{\mathbf{B}}_{ms}^T \bar{D}_{mms}\bar{\mathbf{B}}_{ms}\mathrm{d}\Omega \\
\mathbf{M} &= \int_\Omega \bar{\mathbf{N}}_u^T \bar{\mathbf{m}}\bar{\mathbf{N}}_u\mathrm{d}\Omega;\ \mathbf{q} = \bar{\mathbf{q}}\mathrm{e}^{i\omega t}
\end{aligned} \quad (43)$$

Here, ω represents the natural frequency, while $\bar{\mathbf{q}}$ denotes the mode shapes. Meanwhile, $\mathbf{K}$ and $\mathbf{M}$ denote the global stiffness matrix and mass matrix, respectively.

4. Numerical results

To begin with, we examine square MEE sandwich plates with the materials are outlined in reference [33] to validate the precision and agreement of the proposed model. The material characteristics of the FG-CNTRC core and MEE face sheets are presented in Table 2 and Table 3, respectively.

Tab. 2: The material properties of the FG-CNTRC core.

Properties	Matrix	CNTs
		$E_{11}^{CNT} = 5646.7$
Elastic (GPa)	$E_m = 2.61$	$E_{22}^{CNT} = 7120.5$
		$G_{12}^{CNT} = 1944.5$
Poisson's ratio	$\nu_m = 0.34$	$\nu_{12}^{CNT} = 0.175$
Density (kg/m3)	$\rho_m = 1200$	$\rho^{CNT} = 1400$

Tab. 3: The material parameters of the MEE face sheets.

Properties	$BaTiO_3$-$CoFe_2O_4$
Elastic (GPa)	$c_{11} = c_{22} = 226$; $c_{12} = 125$; $c_{13} = 124$; $c_{33} = 216$; $c_{44} = c_{55} = 44.2$; $c_{66} = 50.5$;
Piezoelectric (Cm-2)	$e_{31} = e_{32} = -2.2$; $e_{33} = 9.3$; $e_{15} = 5.8$
Piezomagnetic (N/Am)	$q_{15} = q_{24} = 275$; $q_{31} = q_{32} = 290.1$; $q_{33} = 349.9$
Dielectric ($10^{-9}C^2m^{-2}N^{-1}$)	$k_{11} = k_{12} = 5.64$; $k_{33} = 6.35$
Magnetic ($10^{-6}Ns^2/C^2$)	$\mu_{11} = \mu_{12} = -297; \mu_{13} = 83.5$
Magnetoelectric ($10^{-12}Ns/VC$)	$d_{11} = d_{12} = 5.367; d_{33} = 2737.5$
Density (kg/m^3)	$\rho^f = 5500$

The boundary conditions consist of a combination of simply supported (S) and clamped (C) edges. Table 4 presents the lowest four natural frequencies of the SSSS sandwich plate with MEE face layers and FG-CNTRC core with different CNTs distributions. The plate is modeled with 9×9, 11×11 and 13×13 meshes. The length scale parameters are neglected (l =0) in this case. The results are compared with those given in [33]. Moreover, it showed a good agreement with the published solution. Besides, the differences between the mesh levels are negligible. Therefore, the forthcoming analysis will use an 11×11 element mesh. Next, Table 5 present the first five dimensionless natural frequency $\overline{\omega} = \omega h\sqrt{\rho_1/E_1}$ of the SSSS metal foam microplates with uniform porosity distribution. The material properties of the metal foam microplate are taken by [34]: $E_1 = 200GPa$, $\nu_1 = 0.33$, $\rho_1 = 7850kg/m^3$. The numerical results are compared with the reference given in ref. [34], which are used the combination of

RPT with four variables, MSGT and IGA. As we see from Table 5, the present calculation results are in good agreement with the published ones. The comparison results in Table 4 and Table 5 present the precision and agreement of the proposed method.

Tab. 4: The lowest four vibrational frequencies of the SSSS MEE sandwich square plate ($a = 20h, l = 0, h_c = 8h_f, V^* = 0.12, \phi_0 = 0, \psi_0 = 0$).

Mode	Theory	Mesh	CNTs distribution		
			FG-X	FG-V	FG-O
1	Ref. [33]		1666.6	1608.3	1585.2
	Present	9×9	1659.5	1581.6	1496.5
		11×11	1659.5	1581.6	1496.5
		13×13	1659.5	1581.6	1496.5
2	Ref. [33]		3475.6	3467.1	3466.9
	Present	9×9	3527.9	3484.9	3440.8
		11×11	3527.7	3484.7	3440.6
		13×13	3257.7	3484.6	3440.6
3	Ref. [33]		3921.4	3744.2	3664.1
	Present	9×9	3934.3	3786.8	3598.0
		11×11	3934.1	3786.7	3597.9
		13×13	3934.1	3786.6	3597.8
4	Ref. [33]		5278.5	5204.6	5177.0
	Present	9×9	5231.3	5102.9	4947.9
		11×11	5231.1	5102.8	4947.6
		13×13	5231.0	5102.7	4947.6

Tab. 5: The lowest five vibrational frequencies of the SSSS metal foam microplate with uniform porosity distribution ($a = 10h, l = 0$).

l/h	Theory	Mode				
		1	2	3	4	5
0	Ref. [34]	0.0562	0.1340	0.1340	0.2054	0.2502
	Present	0.0562	0.1340	0.1340	0.2054	0.2502
0.1	Ref. [34]	0.0601	0.1434	0.1436	0.2203	0.2683
	Present	0.0601	0.1434	0.1436	0.2203	0.2683
0.2	Ref. [34]	0.0706	0.1684	0.1689	0.2595	0.3160
	Present	0.0706	0.1684	0.1689	0.2595	0.3160
0.5	Ref. [34]	0.1203	0.2867	0.2892	0.4447	0.5389
	Present	0.1203	0.2867	0.2892	0.4447	0.5389
1	Ref. [34]	0.2196	0.5225	0.5290	0.8128	0.9813
	Present	0.2196	0.5225	0.5290	0.8128	0.9813

Moving forward, the free vibration analysis of the sandwich microplates with MEE face layers and FG-CNTRC core is investigated. The material parameters of the microplates are taken in Table 2 and Table 3. Besides, the LSPs are taken the same $l_1 = l_2 = l_3 = l$. The first four normalized natural frequencies $\bar{\omega} = \frac{\omega a^2}{h}\sqrt{\frac{\rho_m}{E_m}}$ of the square microplates with FG-CNTRC core and MEE face layers under the effect of the scale-to-thickness ratio (l/h) and CNTs distributions are presented in Table 6. According to this table, the vibrational frequency of the MEE sandwich microplates is decreased with a growth of the parameter l/h. Furthermore, the highest natural frequency is found in the FG-X distribution, followed by FG-UD, FG-V and FG-O configurations. The influence of the external electric potential (ϕ_0) and magnetic potential (ψ_0) on the first normalized frequency of the SSSS and CCCC MEE microplate is studied and plotted in Figure 2 and Figure 3, respectively. As we see in Figure 2 and Figure 3, with a rise of the parameter ϕ_0, the microplate's frequency is decreases. Meanwhile there is a growth of the microplate's frequency with an increase of the parameter ψ_0. The first dimensionless natural frequency of the MEE sandwich microplates with various values of the parameter a/h and CNTs volume fraction (V_s) are presented in Figure 4. It can be seen that in Figure 4, rise in the parameter a/h and CNTs volume fraction leads to the growth of the microplate's natural frequency.

In addition, to show the advantage of the present method, the free vibration of the MEE sandwich circular microplate with radius R is studied. The first four dimensionless natural frequencies $\bar{\omega}_c = \frac{\omega R^2}{h}\sqrt{\frac{\rho_m}{E_m}}$ of the circular microplates with FG-CNTRC core and MEE face layers with various values of parameter l/h and CNTs distributions are tabulated in Table 7. The results in Table 7 show that an increase in the scale-to-thickness ratio leads to a rise in the microplate's frequency. Besides, the FG-X distribution provides the largest vibrational frequency, while the FG-O distribution provides the smallest.

5. Conclusions

The size-dependent free vibration of the sandwich microplates with the MEE face sheets and FG-CNTRC core is studied in this investigation. The RPT and MSGT are employed to derive the governing equation of the MEE sandwich microplates. After that, the IGA is used to solve this governing equation. The impact of various parameters of the material and microplate's

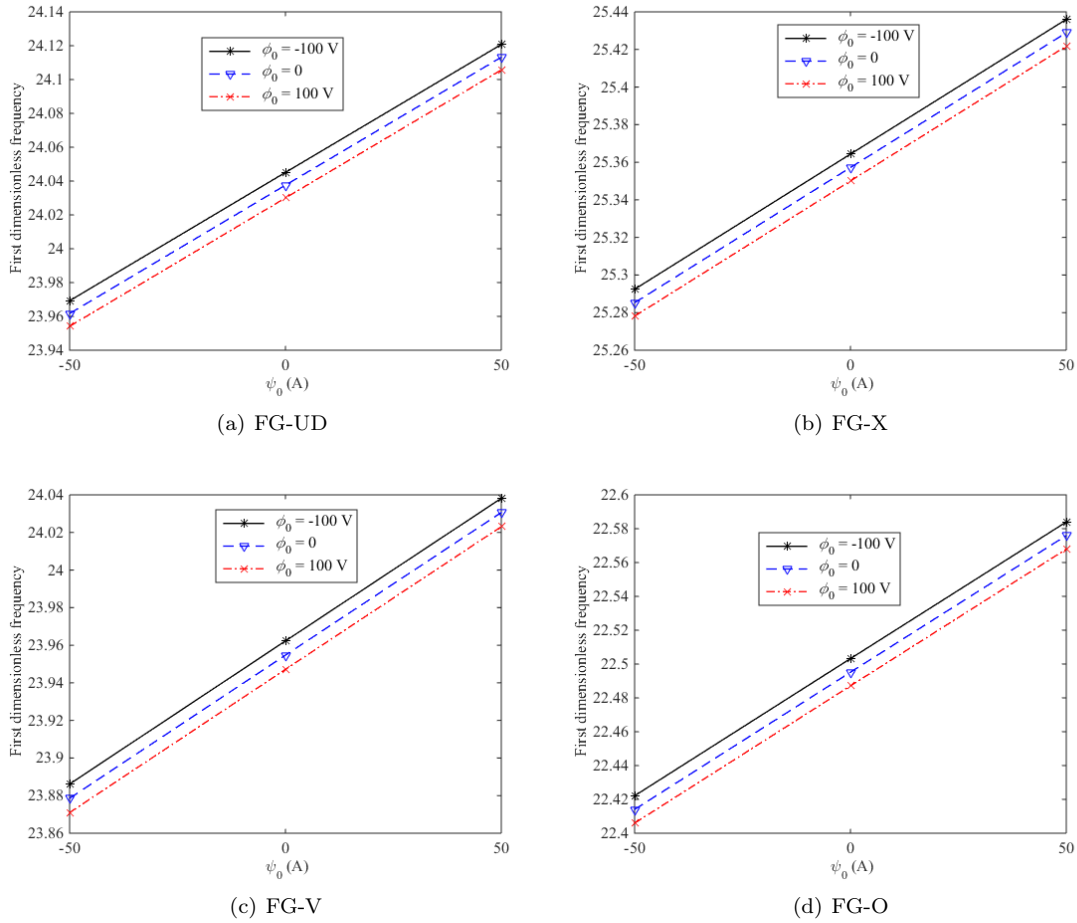

(a) FG-UD (b) FG-X

(c) FG-V (d) FG-O

Fig. 2: The impact of the parameters ϕ_0 and ψ_0 on the first normalized natural frequency of the MEE sandwich square microplate with SSSS boundaries ($a/h = 30, h_c/h_f = 8, V^* = 0.17, l = 0.2h$).

geometry is examined. The results show that a rise in the magnetic potential and electric voltage leads to the improvement and reduction of the sandwich microplate with MEE face sheets. Besides, the microplate's stiffness is enriched with a growth in the length scale parameter. The increase in the CNTs' volume fraction rises the MEE sandwich microplate's frequency. Among the CNTs distributions, the FG-X distribution provides the highest stiffness of the sandwich microplate, followed by FG-UD, FG-V and FG-O distributions. Finally, the growth in the length-to-thickness ratio makes the sandwich microplate stiffer.

Acknowledgment

This work belongs to the project in 2024 funded by Ho Chi Minh City University of Technology and Education, Vietnam.

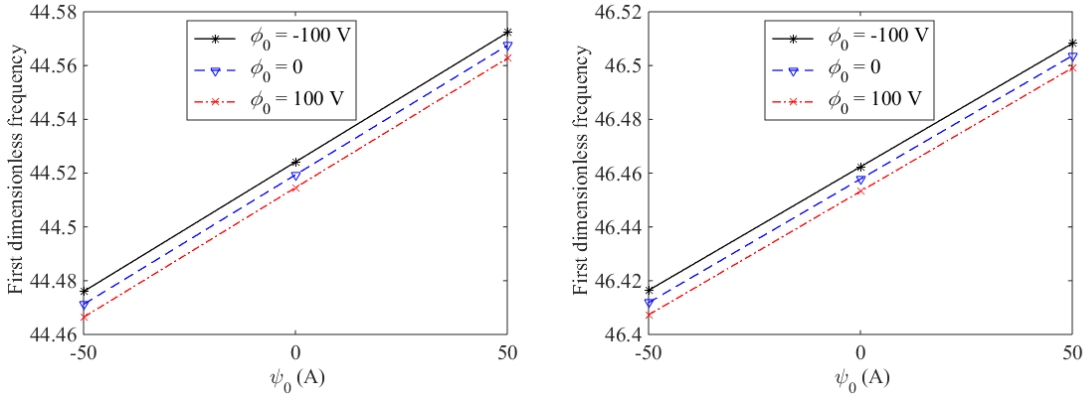

(a) FG-UD (b) FG-X

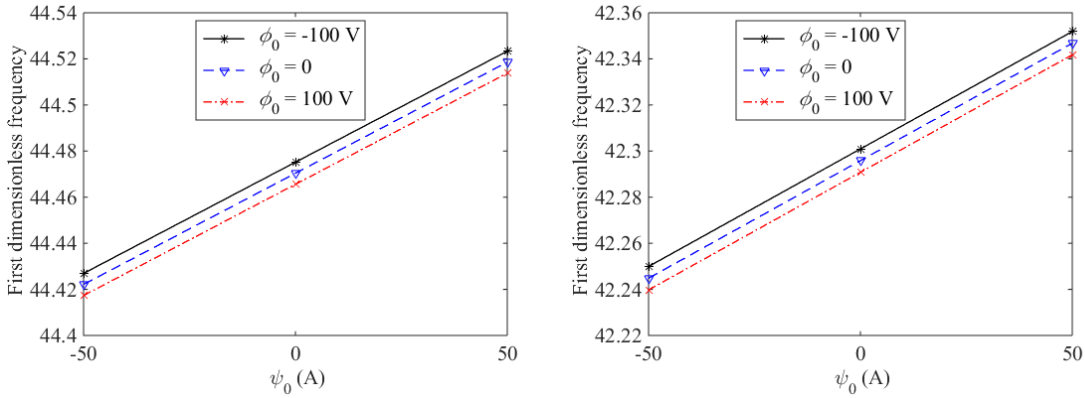

(c) FG-V (d) FG-O

Fig. 3: The impact of the parameters ϕ_0 and ψ_0 on the first normalized natural frequency of the MEE sandwich square microplate with CCCC boundaries ($a/h = 30, h_c/h_f = 8, V^* = 0.17, l = 0.2h$).

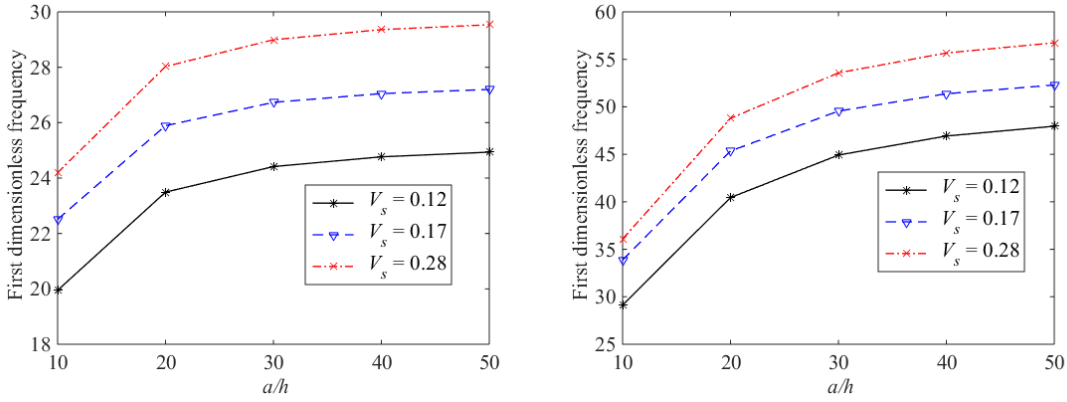

(a) SSSS (b) CCCC

Fig. 4: The effect of the parameter a/h on the first normalized natural frequency of the MEE sandwich square microplate ($h_c/h_f = 8, l = 0.6h, \phi_0 = \psi_0 = 0$).

Tab. 6: The lowest four normalized frequencies of the MEE square sandwich microplate ($a/h = 10, h_c/h_f = 8, V^* = 0.12, \phi_0 = \psi_0 = 0$).

BCs	l/h	Mode	CNTs distribution			
			FG-UD	FG-X	FG-V	FG-O
SSSS	0	1	17.3150	17.7345	17.2995	16.7736
		2	33.9145	33.9293	33.9253	33.7066
		3	34.1403	34.4142	34.1521	33.9165
		4	45.2100	45.2994	45.2289	45.0664
	0.1	1	17.4049	17.8375	17.3899	16.8523
		2	34.1225	34.1571	34.1349	33.9600
		3	34.4293	34.7400	34.4434	34.1073
		4	45.5847	45.7125	45.6064	45.4055
	0.3	1	18.0795	18.6028	18.0680	17.4491
		2	35.6989	35.8752	35.7229	35.5601
		3	36.5877	37.1649	36.6174	35.8591
		4	48.4062	48.8132	48.4481	47.9681
	0.5	1	19.2469	19.9000	19.2406	18.5064
		2	38.4820	38.8760	38.5241	38.1519
		3	40.2677	41.2680	40.3191	39.1256
		4	53.3145	54.1664	53.3865	52.4615
CCCC	0	1	23.4586	23.5171	23.4703	23.3776
		2	39.0980	39.0466	39.1239	39.1414
		3	39.5359	39.3742	39.5652	39.7667
		4	50.6974	50.5180	50.7336	50.9365
	0.1	1	23.6559	23.7339	23.6692	23.5572
		2	39.5098	39.4933	39.5391	39.5207
		3	39.8778	39.7399	39.9097	40.0885
		4	51.2212	51.0790	51.2616	51.4277
	0.3	1	25.1194	25.3390	25.1434	24.8903
		2	42.4180	42.4546	42.4690	42.3514
		3	42.5834	42.8250	42.6371	42.4802
		4	55.1290	55.2625	55.1990	55.0903
	0.5	1	27.6079	28.0541	27.6477	27.1684
		2	46.7798	47.0993	46.8605	46.5971
		3	47.8513	48.5217	47.9412	47.2055
		4	61.8504	62.4426	61.9656	61.3937

Tab. 7: The lowest four normalized frequencies of the MEE circular sandwich microplate ($a/h = 10, h_c/h_f = 6, V^* = 0.12, \phi_0 = \psi_0 = 0$).

BCs	l/h	Mode	CNTs distribution			
			FG-UD	FG-X	FG-V	FG-O
SS	0	1	6.4009	6.6295	6.3913	6.1370
		2	14.3893	14.5533	14.3819	14.2038
		3	15.1914	15.6658	15.1807	14.6057
		4	22.9747	23.3611	22.9637	22.5030
	0.1	1	6.4122	6.6418	6.4026	6.1476
		2	14.4241	14.5908	14.4169	14.2364
		3	15.2364	15.7175	15.2261	14.6452
		4	23.0507	23.4458	23.0402	22.5718
	0.3	1	6.4995	6.7364	6.4905	6.2299
		2	14.6945	14.8815	14.6893	14.4909
		3	15.5811	16.1103	15.5730	14.9498
		4	23.6374	24.0957	23.6311	23.1057
	0.5	1	6.6623	6.9098	6.6542	6.3859
		2	15.2010	15.4202	15.1993	14.9723
		3	16.2028	16.8075	16.1983	15.5093
		4	24.7154	25.2757	24.7162	24.0988
CC	0	1	10.2082	10.4192	10.2043	9.9612
		2	18.4446	18.5643	18.4446	18.3158
		3	18.9091	19.2352	18.9070	18.4925
		4	26.7318	26.9748	26.7319	26.4351
	0.1	1	10.2396	10.4541	10.2360	9.9898
		2	18.5055	18.6304	18.5060	18.3724
		3	18.9875	19.3235	18.9860	18.5621
		4	26.8458	27.1003	26.8469	26.5394
	0.3	1	10.4804	10.7201	10.4784	10.2099
		2	18.9752	19.1385	18.9793	18.8104
		3	19.5844	19.9941	19.5874	19.0938
		4	27.7166	28.0563	27.7243	27.3363
	0.5	1	10.9180	11.1977	10.9189	10.6152
		2	19.8390	20.0656	19.8494	19.6220
		3	20.6522	21.1823	20.6621	20.0550
		4	29.2905	29.7722	29.3090	28.7868

References

[1] D. C. Lam, F. Yang, A. Chong, J. Wang, and P. Tong. Experiments and theory in strain gradient elasticity. *J. Mech. Phys. Solids*, 51:1477–1508, 2003.

[2] Y. Li and W. Feng. Microstructure-dependent piezoelectric beam based on modified strain gradient theory. *Smart materials structures*, 23:095004, 2014.

[3] M. Mohammadi, M. Fooladi, and H. Darijani. Exact boundary conditions for buckling analysis of rectangular micro-plates based on the modified strain gradient theory. *Int. J. for Multiscale Comput. Eng.*, 13:265–280, 2015.

[4] M. Hosseini, M. Bahreman, and A. Jamalpoor. Using the modified strain gradient theory to investigate the size-dependent biaxial buckling analysis of an orthotropic multi-microplate system. *Acta Mech.*, 227:1621–1643, 2016.

[5] A. Karamanli and T. P. Vo. A quasi-3d theory for functionally graded porous microbeams based on the modified strain gradient theory. *Compos. Struct.*, 257:113066, 2021.

[6] Y. Q. Wang, H. L. Zhao, C. Ye, and J. W. Zu. A porous microbeam model for bending and vibration analysis based on the sinusoidal beam theory and modified strain gradient theory. *Int. J. Appl. Mech.*, 10:1850059, 2018.

[7] B. Zhang, Y. He, D. Liu, L. Shen, and J. Lei. An efficient size-dependent plate theory for bending, buckling and free vibration analyses of functionally graded microplates resting on elastic foundation. *Appl. Math. Model.*, 39:3814–3845, 2015.

[8] A. Ashoori and M. Mahmoodi. A nonlinear thick plate formulation based on the modified strain gradient theory. *Mech. Adv. Mater. Struct.*, 25:813–819, 2018.

[9] T. M. Le, D. Vo, Z. Y. Aung, E. Atroshchenko, T. Q. Bui, and J. Rungamornrat. sogeometric analysis of shear-deformable, in-plane functionally graded microshells by mindlin's strain gradient theory. *Eng. with Comput.*, 40:1397–1430, 2024.

[10] T. M. Le, D. Vo, J. Rungamornrat, and T. Q. Bui. Strain-gradient theory for shear deformation free-form microshells: Governing equations of motion and general boundary conditions. *Int. J. Solids Struct.*, 248:111579, 2022.

[11] D. Vo, Z. Y. Aung, T. M. Le, P. Suttakul, E. Atroshchenko, and J. Rungamornrat. Analysis of planar arbitrarily curved microbeams with simplified strain gradient theory and timoshenko–ehrenfest beam model. *Math. Mech. Solids*, 112:358–390, 2022.

[12] M.-F. Liu and T.-P. Chang. Closed form expression for the vibration problem of a transversely isotropic magneto-electro-elastic plate. *J. Appl. Mech.*, 77:024502, 2010.

[13] A. Shooshtari and S. Razavi. Large amplitude free vibration of symmetrically laminated magneto-electro-elastic rectangular plates on pasternak type foundation. *Mech. Res. Commun.*, 69:103–113, 2015.

[14] M. Mohammadimehr and R. Rostami. Bending, buckling, and forced vibration analyses of nonlocal nanocomposite microplate using TSDT considering MEE properties dependent to various volume fractions of $CoFe_2O_4$-$BaTiO_3$. *J. Theor. Appl. Mech.*, 55:853–868, 2017.

[15] K. K. Zur, M. Arefi, J. Kim, and J. N. Reddy. Free vibration and buckling analyses of magneto-electro-elastic fgm nanoplates based on nonlocal modified higher-order sinusoidal shear deformation theory. *Compos. Part B: Eng.*, 182:107601, 2020.

[16] Y.-F. Zheng, L.-L. Xu, and C.-P. Chen. Nonlinear bending analysis of magnetoelectroelastic rectangular plates using higher order shear deformation theory. *J. Mech. Sci. Technol.*, 35:1099–1108, 2021.

[17] Z. Shi, X. Yao, F. Pang, and Q. Wang. An exact solution for the free-vibration analysis of functionally graded carbon-nanotube-reinforced composite beams with arbitrary boundary conditions. *Sci. reports*, 7:12909, 2017.

[18] H. Chalak, A. Zenkour, and A. Garg. Free vibration and modal stress analysis of fg-cntrc beams under hygrothermal conditions using zigzag theory. *Mech. Based Des. Struct. And Mach.*, 51:4709–4730, 2023.

[19] S. Zghal, A. Frikha, and F. Dammak. Static analysis of functionally graded carbon nanotube-reinforced plate and shell structures. *Compos. Struct.*, 176:1107–1123, 2017.

[20] N. D. Duc and P. P. Minh. Free vibration analysis of cracked fg cntrc plates using phase field theory. *Aerosp. Sci. Technol.*, 112:106654, 2021.

[21] T. J. Hughes, J. A. Cottrell, and Y. Bazilevs. Isogeometric analysis: Cad, finite elements, nurbs, exact geometry and mesh refinement. *Comput. methods applied mechanics engineering*, 194:4135–4195, 2005.

[22] C. H. Thai, A. Ferreira, and H. Nguyen-Xuan. Isogeometric analysis of size-dependent isotropic and sandwich functionally graded microplates based on modified strain gradient elasticity theory. *Compos. Struct.*, 192:274–288, 2018.

[23] C. H. Thai, A. Ferreira, and P. Phung-Van. Size dependent free vibration analysis of multilayer functionally graded gplrc microplates based on modified strain gradient theory. *Compos. Part B: Eng.*, 169:174–188, 2019.

[24] C. H. Thai, A. Ferreira, T. Rabczuk, and H. Nguyen-Xuan. Size-dependent analysis of fg-cntrc microplates based on modified strain gradient elasticity theory. *Eur. J. Mech.*, 72:521–538, 2018.

[25] C. H. Thai, T. Tran, and P. Phung-Van. A size-dependent moving kriging meshfree model for deformation and free vibration analysis of functionally graded carbon nanotube-reinforced composite nanoplates. *Eng. Anal. with Bound. Elem.*, 115:52–63, 2020.

[26] C. H. Thai and H. Nguyen-Xuan. A simple size-dependent isogeometric approach for bending analysis of functionally graded microplates using the modified strain gradient elasticity theory. *Vietnam. J. Mech.*, 42:255–267, 2020.

[27] S. K. Singh and I. V. Singh. Extended isogeometric analysis for fracture in functionally graded magneto-electro-elastic material. *Eng. Fract. Mech.*, 247:107640, 2021.

[28] R. Kiran, N. Nguyen-Thanh, H. Yu, and K. Zhou. Adaptive isogeometric analysis–based phase-field modeling of interfacial fracture in piezoelectric composites. *Eng. Fract. Mech.*, 228:109181, 2023.

[29] R. Kiran, N. Nguyen-Thanh, and K. Zho. Adaptive isogeometric analysis–based phase-field modeling of brittle electromechanical fracture in piezoceramics. *Eng. Fract. Mech.*, 274:108738, 2022.

[30] L.-L. Ke and Y.-S. Wang. Free vibration of size-dependent magneto-electro-elastic nanobeams based on the nonlocal theory. *Phys. E: Low-Dimensional Syst. Nanostructures*, 63:52–61, 2014.

[31] M. Mohammadimehr, S. Okhravi, and S. Akhavan Alavi. Free vibration analysis of magneto-electro-elastic cylindrical composite panel reinforced by various distributions of cnts with considering open and closed circuits boundary conditions based on fsdt. *J. Vib. Control.*, 24:1551–1569, 2018.

[32] A. Sofiyev, B. E. Turkaslan, R. Bayramov, and M. Salamci. Analytical solution of stability of fg-cntrc conical shells under external pressures. *Thin-Walled Struct.*, 144:106338, 2019.

[33] N. D. Dat, T. Q. Quan, V. Mahesh, and N. D. Duc. Analytical solutions for nonlinear magneto-electro-elastic vibration of smart sandwich plate with carbon nanotube reinforced nanocomposite core in hygrothermal environment. *Int. J. Mech. Sci.*, 186:105906, 2020.

[34] P. T. Hung, P. Phung-Van, and C. H. Thai. A refined isogeometric plate analysis of porous metal foam microplates using modified strain gradient theory. *Compos. Struct.*, 289:115467,, 2022.

About Authors

T. T. TRIEN was born in Vietnam in 1982. He has a Master. degree in Mechanics. Now, he is a lecturer at the Faculty of Civil Engineering at Ho Chi Minh City University of Technology and Education, Ho Chi Minh City, Vietnam. His research interests are the computational mechanics. Email address: trientt@hcmute.edu.vn.

P. H. HUNG was born in Vietnam in 1981. He has a Ph.D. degree in Mechanics. Now, he is a lecturer at the Faculty of Civil Engineering at Ho Chi Minh City University of Technology and Education, Ho Chi Minh City, Vietnam. His research interests are the computational mechanics. Email address: hungpht@hcmute.edu.vn.

